A&A, 708, A182 (2026)
https://doi.org/10.1051/0004-6361/202557134

Astronomy & Astrophysics

Detectability of continuous gravitational waves from planetary-mass companions orbiting compact stars

Abdusattar Kurban[1,2,3,⋆], Xia Zhou[1,2,3], Na Wang[1,2,3], Yong-Feng Huang[4,5], Wenming Yan[1,2,3], Jianping Yuan[1,2,3], Ali Esamdin[3], Yu-Bin Wang[6], Zhigang Wen[1,2,3], and Rai Yuen[1,2,3]

[1] State Key Laboratory of Radio Astronomy and Technology, Xinjiang Astronomical Observatory, CAS, 150 Science 1-Street, Urumqi, Xinjiang, 830011, PR China
[2] Xinjiang Key Laboratory of Radio Astrophysics, Urumqi, Xinjiang, 830011, PR China
[3] Xinjiang Astronomical Observatory, Chinese Academy of Sciences, Urumqi, Xinjiang 830011, PR China
[4] School of Astronomy and Space Science, Nanjing University, Nanjing 210023, PR China
[5] Key Laboratory of Modern Astronomy and Astrophysics (Nanjing University), Ministry of Education, Nanjing 210023, PR China
[6] School of Physics and Electronic Engineering, Sichuan University of Science & Engineering, Zigong 643000, PR China

Received 7 September 2025 / Accepted 15 February 2026

ABSTRACT

Binary systems with ultrashort-period planetary-mass companions are expected to radiate continuous gravitational waves (GWs). However, earlier studies found that the detectability of such systems by the Laser Interferometer Space Antenna (LISA) is unlikely. In this study, we investigate the detectability of GWs from planetary-mass companions orbiting pulsars (PSRs) or white dwarfs (WDs) whose fundamental parameters, essential for calculating GW properties, have been measured. We compare the GW signals from our sample with the sensitivity curves of space-based GW detectors. We find that fourteen sources achieve a signal-to-noise ratio (S/N) of $\gtrsim 5$ within four years of observations. Among these, three sources have PSR primaries (2S 0918-549 b, 4U 0513-40 b, and 4U 1543-62), and eleven systems possess WD primaries (BW Scl b, CP Eri b, CR Boo b, EF Eri b, GP Com b, GW Lib b, SDSS J0926+3624 b, SDSS J1507+5230 b, SMSS J1606-1000 b, SRGeJ0453 b, and WZ Sge b). We note that their detectability is less probable with near-term missions such as LISA, TianQin, and Taiji. Nevertheless, they could be detected by more advanced, future-generation observatories, such as the Deci-hertz Interferometer Gravitational wave Observatory (DECIGO) and the Big Bang Observer (BBO). This offers the potential to investigate the formation and evolution of ultrashort-period planetary-mass companions around compact stars through joint GW and electromagnetic surveys.

Key words. planets and satellites: general – planet–star interactions

1. Introduction

The direct detection of gravitational waves (GWs) from binary black hole mergers (Abbott et al. 2016) and a binary neutron star inspiral (Abbott et al. 2017) by ground-based GW detectors operating in high-frequency bands has opened a new window for observing the Universe. Space-based GW detectors such as the Laser Interferometer Space Antenna (LISA; Amaro-Seoane et al. 2017), TianQin (Luo et al. 2016), and Taiji (Ruan et al. 2020) aim to detect GW signals in the milli-hertz frequency band, which are inaccessible to ground-based detectors. LISA is an approved mission with well-defined design sensitivity, whereas TianQin and Taiji are in the advanced stages of planning. The scientific objectives of these instruments encompass the investigation of various compact binary systems and the stochastic GW background of astrophysical origin (Ruan et al. 2020; Huang et al. 2020; Amaro-Seoane et al. 2023).

In addition to the aforementioned instruments, proposed far-future space-based GW detectors such as the Deci-hertz Interferometer Gravitational wave Observatory (DECIGO; Kawamura et al. 2006) and the Big Bang Observer (BBO; Harry et al. 2006) are designed to investigate events within the deci-hertz range of GW frequencies. The projected sensitivities of these two conceptual detectors are several orders of magnitude superior to those of LISA, TianQin, and Taiji, aiming to explore the early Universe and compact objects (Cutler & Harms 2006; Yagi & Seto 2011). The studies based on these space-based GW instruments are expected to provide a more comprehensive understanding of the formation and evolution of compact binary systems and to trace the merger history of compact objects through GW astronomy.

Ultracompact binaries with orbital periods less than 60 minutes have been proposed as potential GW sources for the LISA mission due to their strong GW signals (Kupfer et al. 2018; Burdge et al. 2020). These systems consist of a white dwarf (WD) or neutron star (NS) primary and a compact helium-star, WD, or NS secondary. Kupfer et al. (2018) argued that, assuming an optimistic 10-year mission for LISA, some ultracompact binaries can produce a signal-to-noise ratio (S/N) greater than 5; they are referred to as LISA verification binaries and include AM Canum Venaticorum (AM CVn) systems, double WDs, subdwarf B-star systems, and ultracompact X-ray binaries (UCXBs). Subsequent studies have shown that a subclass of UCXBs is detectable by LISA with a considerable S/N (Chen et al. 2020; Yu et al. 2021; Suvorov 2021; Chen & Liu 2025).

It has been proposed that some special planetary-mass companions orbiting pulsars (PSRs) could serve as potential GW sources for upcoming GW detectors. For instance, small planetary-mass objects in close orbits around PSRs might belong to strange quark matter planetary systems

⋆ Corresponding author: akurban@xao.ac.cn

(Huang & Yu 2017; Kuerban et al. 2020; Zhang et al. 2024a). The strong GW bursts produced during the final inspiral stage of such systems within our Galaxy could potentially be detected by future ground-based GW detectors (Geng et al. 2015; Kuerban et al. 2019; Zhang et al. 2024b).

Previous studies have highlighted that continuous GWs from binary systems with ultrashort period planetary-mass companions, such as GP Com b, could be particularly interesting targets for the LISA mission (Cunha et al. 2018). However, Wong et al. (2019) demonstrated that observing this system for four years would not produce an S/N sufficient for detection by LISA, suggesting that detecting such systems is less likely. In recent years, the number of confirmed extrasolar planetary-mass companions has increased significantly. Additionally, except for LISA, other space-based GW detectors with different sensitivities, such as TianQin, Taiji, DECIGO, and BBO, are also planned. Based on the sensitivity characteristics of these detectors, we probe the gravitational-wave signatures of short-period planetary-mass companions orbiting compact stars using the most up-to-date data.

The structure of this paper is organized as follows. The theoretical GW signal model is presented in Section 2. The parameters of our planetary-mass companions orbiting compact stars are given in Section 3. The characteristics of the GW signal produced by our selected samples are presented in Section 4. Finally, Section 5 presents our conclusions and some brief discussions.

2. GW signal model

For a binary system in a circular orbit composed of a primary mass m_1 and a companion mass m_2, the power of emitted GW radiation can be expressed as (Peters & Mathews 1963)

$$P = \frac{32}{5}\frac{G^{7/3}}{c^5}(2\pi f_{\rm orb}\mathcal{M}_c)^{10/3}, \tag{1}$$

where G is the gravitational constant, c is the speed of light, $\mathcal{M}_c = (m_1 m_2)^{3/5}/(m_1+m_2)^{1/5}$ is the chirp mass, and $f_{\rm orb}$ is the orbital frequency related to the orbital period by the equation $f_{\rm orb} = 1/P_{\rm orb}$. For a source at a luminosity distance D_L, the strain amplitude of GW is (e.g., Wagg et al. 2022)

$$h_0 = \frac{8}{\sqrt{5}}\frac{(G\mathcal{M}_c)^{5/3}}{c^4 D_L}(2\pi f_{\rm orb})^{2/3}. \tag{2}$$

The GW frequency can be estimated by

$$f_{\rm gw} = 2 f_{\rm orb}. \tag{3}$$

Its change rate due to the GW radiation is

$$\dot{f}_{\rm gw} = \frac{96}{5\pi}\frac{(G\mathcal{M}_c)^{5/3}}{c^5}(2\pi f_{\rm orb})^{11/3}. \tag{4}$$

The GW signal from a binary system spends approximately $\Delta T = f_{\rm gw}/\dot{f}_{\rm gw}$ seconds in the vicinity of a frequency $f_{\rm gw}$, which leads to the signal accumulating at the frequency $f_{\rm gw}$ (Finn & Thorne 2000). The accumulated signal represents the characteristic strain amplitude, h_c, which can be related to h_0 as (e.g., Finn & Thorne 2000; Moore et al. 2015)

$$h_c = h_0\sqrt{N_{\rm cycle}} = h_0\sqrt{\frac{f_{\rm gw}^2}{\dot{f}_{\rm gw}}} = h_0\sqrt{f_{\rm gw}\Delta T}. \tag{5}$$

A binary system can be regarded as a stationary source when $\dot{f}_{\rm gw} < 1/T_{\rm obs}^2$, where $T_{\rm obs}$ is the observation duration. For such systems with $T_{\rm obs} < \Delta T$, the characteristic strain can be estimated as

$$h_c = h_0\sqrt{f_{\rm gw}T_{\rm obs}}. \tag{6}$$

Let us consider the noise power spectral density for a GW detector, denoted as $S_{\rm n}(f_{\rm gw})$. The noise characteristic amplitude corresponding to h_c can be expressed as $S_h = \sqrt{f_{\rm gw}S_{\rm n}(f_{\rm gw})}$. In the case of a stationary and circular binary system, the fully averaged S/N (acquired by averaging the S/N across position, inclination, and polarization; Wagg et al. (2022)) is presented as

$$S/N = \frac{h_c}{S_h} = \sqrt{\frac{h_0^2 T_{\rm obs}}{S_{\rm n}(f_{\rm gw})}}. \tag{7}$$

In subsequent sections, the GW characteristics of our sample are calculated using these equations.

3. Sample selection

The data of the binary systems with planetary-mass companions considered in this work were taken from the Exoplanetary Systems Encyclopaedia catalog[1] (Schneider et al. 2011). To date, more than 7000 exoplanets confirmed through electromagnetic observations have been cataloged in this database. Computing the GW properties of binary systems hinges on fundamental parameters such as companion mass, primary mass, orbital period (or semimajor axis), and our distance to the source. Therefore, we selected the sources for which these parameters have been documented in the catalog. We are particularly interested in the sources whose GW frequency lie within the frequency range of space-based GW instruments. Planetary-mass companions with orbital periods $P_{\rm orb} < 0.07$ days are expected to produce continuous GWs at this frequency range and can be potential targets for space-based GW detectors. Interestingly, the systems selected in this manner are specifically found to consist of planetary-mass objects orbiting around PSRs and WDs (i.e., PSR systems and WD systems). The details of these systems are listed in Table A.1.

Note that the classification of these companions in our samples as planets is still a matter of ongoing debate. This is because they exhibit a mass range extending from approximately 1 to 80 Jupiter mass ($M_{\rm Jup}$). Objects within this mass range could be either brown dwarfs or giant planets. Brown dwarfs typically possess masses that fall between the deuterium fusion threshold of 13 $M_{\rm Jup}$ (Spiegel et al. 2011) and the hydrogen fusion threshold of 80 $M_{\rm Jup}$ (Grieves et al. 2021). There has been debate regarding the upper mass boundary for planets, which could be 25 $M_{\rm Jup}$ (Schneider et al. 2011) or 60 $M_{\rm Jup}$ (Hatzes & Rauer 2015). It has also been posited that 42.5 $M_{\rm Jup}$ represents the transitional boundary between giant planets and brown dwarfs (Ma & Ge 2014).

4. Results

The GW characteristics of the samples selected in Section 3 were calculated using the signal model presented in Section 2. Our calculations were performed under the assumption that these

[1] https://exoplanet.eu/catalog/

systems are stationary and their orbits are circular. First, we verified the stationarity by checking the condition $\dot{f}_{\rm gw} < 1/T^2_{\rm obs}$. As shown in Table A.1, $\dot{f}_{\rm gw} \leq 3.81 \times 10^{-18}$ Hz s^{-1} for all samples, which is smaller than $1/T^2_{\rm obs} = 1.57 \times 10^{-17}$ Hz s^{-1} in the case of the longest observation time considered in this work, $T_{\rm obs} = 8$ yr. Additionally, for our samples, the numerical results show that $\Delta T = f_{\rm gw}/\dot{f}_{\rm gw} \geq 1.63 \times 10^7$ yr, which is significantly longer than $T_{\rm obs}$. Therefore, our stationarity assumption is valid for the calculations in this work. As for the eccentricity (e), this parameter is unfortunately unavailable for most systems in the catalog or the relevant literature, except for NGC 6440 X-2 b. For eccentric binary systems, the dominant GW frequency can be evaluated by $f_{\rm gw} = n_{\rm peak}(e) f_{\rm orb}$, where $n_{\rm peak}(e) \approx 2$ when $e \lesssim 0.17$ (Hamers 2021). We notice that NGC 6440 X-2 b has a relatively small eccentricity of $e = 0.07$. In fact, for compact binaries with a small orbital period, the eccentricity is likely to be generally small because the orbit tends to be circularized. Hence, we simply took $n_{\rm peak}(e) = 2$ and adopted $f_{\rm gw} = 2 f_{\rm orb}$ in our calculations. Nevertheless, it should be noted that for sources with an eccentricity of $e > 0.17$, the influence of eccentricity on GW properties should be considered, as in Wagg et al. (2022). Below, we present our numerical results.

4.1. Characteristic strain

Gravitational wave frequency was calculated using Equation (3), while the characteristic strain h_c was calculated using Equation (6). The full possible range of h_c allowed by the parameter uncertainties was evaluated in a conservative approach. The upper and lower bounds of h_c characterizing this potential range were determined by the upper and lower bounds of the strain amplitude h_0, which were calculated by considering the upper and lower bounds of D_L and $\mathcal{M}_c$.

The detectability of the GW signals from sources can be roughly assessed by comparing the characteristic strain of the source with the sensitivity curve of a detector, as discussed in Robson et al. (2019). We obtained the sensitivity curves of LISA (Robson et al. 2019) and TianQin (Huang et al. 2020) using LEGWORK (Wagg et al. 2022). For Taiji, the sensitivity curve was calculated following Liu et al. (2023). The sensitivity curves for DECIGO and BBO were obtained by incorporating the confusion noise contributions from both Galactic and extragalactic compact binaries into the instrumental noise estimates (Yagi & Seto 2011, 2017). This synthesis was performed following the methodology detailed in Sun & Li (2023) and Sun et al. (2024).

The GW signals from our samples, observed over a period of $T_{\rm obs} = 4$ yr, were compared with the sensitivity curves of these detectors in the frequency versus characteristic strain plane, as illustrated in Fig. 1. The figure clearly shows that only a small fraction of our sample exhibits signals that lie above the sensitivity curves of the TianQin, LISA, and Taiji detectors. In stark contrast, a substantial population of sources lies above the sensitivity curves of DECIGO and BBO. However, the actual detectability of these sources, despite their positions above the noise curves, must be assessed based on their S/N values.

4.2. Signal-to-noise ratio

For a source to be considered detectable, its S/N must exceed a certain threshold. For monochromatic systems, this threshold is typically set at S/N = 5 (Kupfer et al. 2018). Here, we define $\mathrm{S/N_{thr}} = 5$ as the detection threshold. Sources satisfying $\mathrm{S/N} \geq \mathrm{S/N_{thr}}$ are deemed detectable.

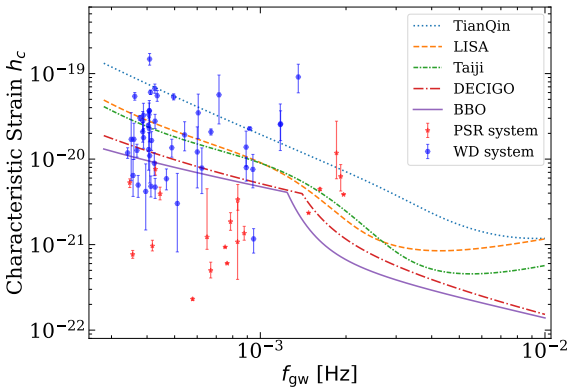

Fig. 1. Comparison of the characteristic strain of our sample with $\sqrt{f_{\rm gw} S_{\rm n}(f_{\rm gw})}$ for $T_{\rm obs} = 4$ yr of observations, where $S_{\rm n}(f_{\rm gw})$ represents the noise power spectral densities for TianQin (dotted line; Huang et al. 2020), LISA (dashed line; Robson et al. 2019), Taiji (densely dashdotted line; Liu et al. 2023), DECIGO (dot-dashed line), and BBO (solid line) (Yagi & Seto 2011; Sun & Li 2023; Sun et al. 2024). The stars and hexagons denote the PSR systems and WD systems, respectively.

For monochromatic sources, the S/N can be estimated from Equation (7), which scales with the square root of the observation time $T_{\rm obs}$. We calculated the S/N for our samples with respect to various detectors, each with different $T_{\rm obs}$. The results are presented in Table A.2. From the table, it is evident that the S/N depends on the detectors, observation duration, and source properties. The S/N of each source lies in a range defined by the upper and lower bounds, computed using the upper and lower bounds of h_0. Here we denote the upper, central, and lower S/N values as $\mathrm{S/N_{up}}$, $\mathrm{S/N_{cen}}$, and $\mathrm{S/N_{low}}$, respectively, which satisfy $\mathrm{S/N_{up}} > \mathrm{S/N_{cen}} > \mathrm{S/N_{low}}$. In Tables A.2 and 1, the potential range of the S/N for a mission is represented by the $\mathrm{S/N_{cen}}$ along with its superscript (defined as $\mathrm{S/N_{up}} - \mathrm{S/N_{cen}}$) and subscript (defined as $\mathrm{S/N_{low}} - \mathrm{S/N_{cen}}$). For instance, the observation of 4U 1543-62 b by TianQin for $T_{\rm obs} = 4$ yr yields an S/N of $1.48^{+2.01}_{-0.74}$. The corresponding $\mathrm{S/N_{up}}$, $\mathrm{S/N_{cen}}$, and $\mathrm{S/N_{low}}$ are 3.49, 1.48, and 0.74, respectively. In this work, we focused on sources with $\mathrm{S/N_{cen}} \gtrsim \mathrm{S/N_{thr}}$ across all considered configurations. We refrained from further analyzing sources whose S/N remained below the detection threshold. As shown in the table, a subset of sources exhibits $\mathrm{S/N_{cen}} \gtrsim \mathrm{S/N_{thr}}$. They are promising candidates for GW detections. Figure 2 plots the S/N of these promising sources for various detectors and observation durations. Below, we analyze the detectability of these promising sources in detail.

4.2.1. Sources with a PSR primary

For the sources with a PSR primary considered here – as depicted in Fig. 2 and Table A.2 – none yield $\mathrm{S/N_{cen}} \gtrsim \mathrm{S/N_{thr}}$ for near-term missions such as TianQin, LISA, and Taiji within an observation duration of $T_{\rm obs} \leq 4$ yr. For far-future conceptual detectors such as DECIGO and BBO, the number of detectable sources markedly increases. When $T_{\rm obs} = 4$ yr, 2S 0918-549 b, 4U 0513-40 b, and 4U 1543-62 are detectable by BBO with $\mathrm{S/N_{low}} > \mathrm{S/N_{thr}}$, while DECIGO detects 4U 1543-62 b with $\mathrm{S/N_{cen}} > \mathrm{S/N_{thr}}$. Among them, 4U 1543-62 b is detectable by BBO within a comparatively shorter observation duration of $T_{\rm obs} = 2$ yr, with $\mathrm{S/N_{cen}} > \mathrm{S/N_{thr}}$. As shown in Fig. 2 and Table A.2, some sets of configurations yield $\mathrm{S/N_{up}} > \mathrm{S/N_{thr}} > \mathrm{S/N_{cen}}$, which indicates marginal detection with the most optimistic S/N values.

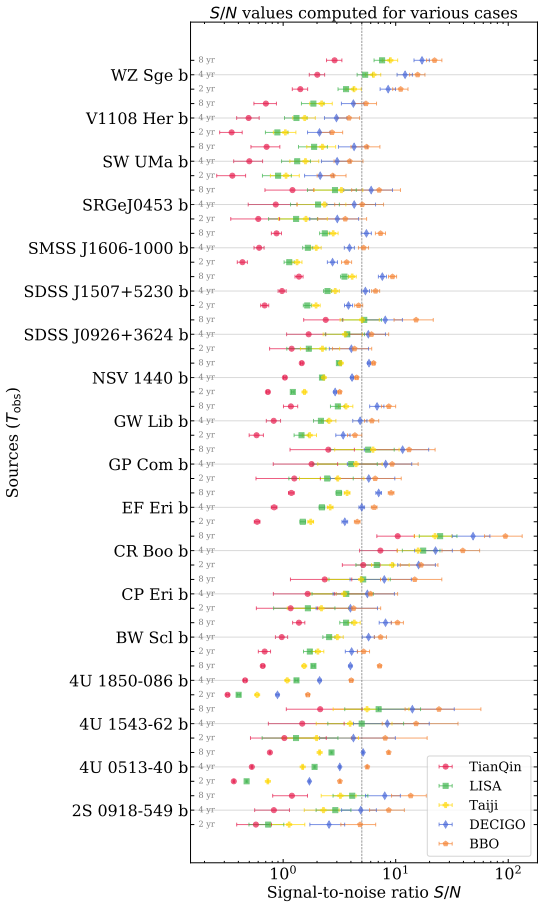

Fig. 2. S/N values of the promising sources for various detectors and observation durations. The circles, squares, filled pluses, rhombuses, and pentagons represent the TianQin, LISA, Taiji, DECIGO, and BBO results, respectively. The data points situated on the horizontal gray line corresponding to each source signify the S/N values calculated for T_{obs} = 4 yr. The S/N values calculated for T_{obs} = 2 yr and T_{obs} = 8 yr are shown in the lower and upper sides of the horizontal gray line, respectively. The vertical dashed gray line denotes S/N_{thr} = 5. Sources with $S/N \gtrsim S/N_{thr}$ are regarded as detectable. Sources with S/N ≥ 1 indicate that the GW signals lie above the sensitivity curves of the corresponding detectors.

4.2.2. Sources with a WD primary

For the sources with a WD primary in our samples, the detectability also depends on the detectors and T_{obs}, as shown in Fig. 2 and Table A.2. For near-term detectors (TianQin, LISA, and Taiji), the number of detectable sources is relatively low. When T_{obs} = 4 yr, CR Boo b and WZ Sge b have signals with $S/N_{cen} \gtrsim S/N_{thr}$ for both LISA and Taiji. But, for TianQin, only CR Boo b has such a strong signal. Nevertheless, an S/N with a lower bound $S/N_{low} < S/N_{thr}$ can be generated by CR Boo b for TianQin and by WZ Sge b for LISA. As shown in Fig. 2 and Table A.2 CP Eri b, GP Com b, and SDSS J0926+3624 b yield $S/N_{up} > S/N_{thr} > S/N_{cen}$ for LISA and Taiji, indicating potential detectability when the most optimistic S/N values are taken into account. When T_{obs} = 2 yr, only CR Boo b yields $S/N_{cen} > S/N_{thr}$ for TianQin, LISA, and Taiji. However, for this source, it is worth noting that $S/N_{low} < S/N_{thr}$ for TianQin and LISA.

For far-future conceptual detectors (DECIGO and BBO), several sources yield a signal with $S/N_{cen} \gtrsim S/N_{thr}$ within T_{obs} = 2 yr or T_{obs} = 4 yr of observations. When T_{obs} = 4 yr, BW Scl b, CP Eri b, CR Boo b, EF Eri b, GP Com b, SDSS J0926+3624 b, SDSS J1507+5230 b, and WZ Sge b are detectable to both DECIGO and BBO, while GW Lib b, SMSS J1606-1000 b, and SRGeJ0453 b are promising targets for BBO only. Among them, the sources reaching the detection threshold S/N_{thr} under T_{obs} = 2 yr are CR Boo b, GP Com b, WZ Sge b (for both DECIGO and BBO), and BW Scl b (for BBO only).

4.2.3. Potential sources and detectability enhancement

In addition to the systems with $S/N_{cen} \gtrsim 5$ discussed above, sources with $5 > S/N_{cen} > 3$ and those marginally detected with the most optimistic S/N values (i.e., $S/N_{up} \gtrsim S/N_{thr} > S/N_{cen}$) also deserve our attention as potential targets for GW detectors. The detectability of these sources can be enhanced through two main methods.

First, extending the mission duration can significantly improve the S/N, thereby increasing the likelihood of detection. A longer observation period allows more signal to accumulate, amplifying the S/N and bringing these sources closer to or above the detection threshold. In our samples, some systems that fail to reach the detection threshold S/N_{thr} for T_{obs} = 4 yr can yield an S/N_{cen} value higher than 5 after being observed for T_{obs} = 8 yr. For systems with a PSR primary, these include 4U 1543-62 b for LISA and Taiji, 2S 0918-549 b and 4U 0513-40 b for DECIGO, and 4U 1850-086 b for BBO. Similarly, for systems with a WD primary, nine sources yield a signal with $S/N_{cen} \gtrsim S/N_{thr}$ after being observed for T_{obs} = 8 yr. They include three systems (CP Eri b, GP Com b, and SDSS J0926+3624 b) for LISA and Taiji, one system (NSV 1440 b) for both DECIGO and BBO, three systems (GW Lib, SMSS J1606-1000 b, and SRGeJ0453 b) for DECIGO, and two systems (SW UMa b and V1108 Her b) for BBO.

Second, the S/N values of such potential sources can be substantially enhanced by network observations. Specifically, the S/N of a source in a joint observation campaign is calculated as the square root of the sum of the squares of the individual S/N values from each detector, i.e., $S/N = \sqrt{\sum S/N_i^2}$ (Wu & Li 2023), where i represents the ith detector of network observations. This enhancement is particularly effective when the individual S/N values are comparable. Table 1 lists the S/N values yielded by individual and combined detector networks. We see that the combined network of detectors can considerably enhance the S/N. For example, independent observations of 4U 1543-62 b by a single detector of TianQin, LISA, and Taiji over an observation period of T_{obs} = 4 yr yield an S/N of $1.48^{+2.01}_{-0.74}$, $4.99^{+6.67}_{-2.49}$, and $3.93^{+5.34}_{-1.97}$, respectively. In comparison, the network observation attains a S/N of $5.20^{+7.06}_{-2.60}$, $4.20^{+5.70}_{-2.10}$, $6.35^{+8.62}_{-3.18}$, and $6.52^{+8.85}_{-3.26}$ for the combined networks TianQin+LISA, TianQin+Taiji, LISA+Taiji, and TianQin+LISA+Taiji, respectively. The table likewise indicates that the S/N_{cen} yielded by most network configurations (TianQin+LISA, LISA+Taiji, and TianQin+LISA+Taiji) exceeds the detection threshold S/N_{thr}. Similarly, for systems with a WD primary, the sources CP Eri b, GP Com b, SDSS J0926+3624 b, and WZ Sge b could serve as potential targets for the combined networks TianQin+LISA, TianQin+Taiji, LISA+Taiji, and/or TianQin+LISA+Taiji. We also notice that $S/N_{thr} > S/N_{low}$ holds for the results obtained from these network observations, suggesting that the parameter uncertainties still considerably influence detectability. We posit that the future DECIGO+BBO network has the potential to further enhance detectability significantly.

Table 1. S/N values of five exemplary sources computed for individual and combined networks using TianQin, LISA, and Taiji, with $T_{\rm obs}$ = 4 yr.

Source	TianQin	LISA	Taiji	TianQin+LISA	TianQin+Taiji	LISA+Taiji	TianQin+LISA+Taiji
4U 1543-62 b	$1.48^{+2.01}_{-0.74}$	$4.99^{+6.67}_{-2.49}$	$3.93^{+5.34}_{-1.97}$	$5.20^{+7.06}_{-2.60}$	$4.20^{+5.70}_{-2.10}$	$6.35^{+8.62}_{-3.18}$	$6.52^{+8.85}_{-3.26}$
CP Eri b	$1.65^{+1.22}_{-0.83}$	$3.64^{+2.69}_{-1.83}$	$3.49^{+2.58}_{-1.76}$	$3.99^{+2.95}_{-2.01}$	$3.86^{+2.85}_{-1.94}$	$5.04^{+3.73}_{-2.54}$	$5.30^{+3.92}_{-2.67}$
GP Com b	$1.79^{+1.26}_{-0.97}$	$4.03^{+2.83}_{-2.19}$	$4.45^{+3.13}_{-2.42}$	$4.41^{+3.10}_{-2.39}$	$4.79^{+3.37}_{-2.61}$	$6.00^{+4.22}_{-3.26}$	$6.26^{+4.41}_{-3.40}$
SDSS J0926+3624 b	$1.68^{+0.71}_{-0.61}$	$3.72^{+1.56}_{-1.35}$	$3.56^{+1.50}_{-1.29}$	$4.08^{+1.72}_{-1.48}$	$3.94^{+1.66}_{-1.43}$	$5.15^{+2.16}_{-1.87}$	$5.42^{+2.28}_{-1.97}$
WZ Sge b	$2.01^{+0.32}_{-0.30}$	$5.35^{+0.86}_{-0.81}$	$6.34^{+1.02}_{-0.96}$	$5.72^{+0.92}_{-0.87}$	$6.65^{+1.07}_{-1.01}$	$8.30^{+1.34}_{-1.26}$	$8.54^{+1.38}_{-1.29}$

Moreover, the detectability of these sources is also influenced by their geometric properties. The sky position, orbital inclination, and polarization angle of a system can affect the S/N by a factor of a few due to the amplitude modulation caused by the detector's orbital motion (Huang et al. 2020; Wagg et al. 2022). Favorable orientations (inclination and polarization angle) and/or advantageous sky locations can enhance the S/N sufficiently to make these sources detectable.

5. Conclusions and discussions

In this study, we investigated the detectability of GWs from planetary-mass objects around compact stars by various space-based GW detectors. We focused on ultrashort-period systems ($P_{\rm orb}$ < 0.07 days) with measured fundamental parameters essential for calculating their GW emission properties. Our samples consisted of systems featuring a PSR primary or a WD primary. We compared the GW signals from our samples to the sensitivity curves of near-term detectors (TianQin, LISA, and Taiji), and next-generation conceptual instruments (DECIGO and BBO) in a characteristic strain versus GW frequency diagram and calculated their S/N values. We find that a subset of these systems is detectable by these GW observatories and summarize our main results below.

For systems with a PSR primary, the sources 2S 0918-549 b, 4U 0513-40 b, and 4U 1543-62 yield a signal with $S/N_{\rm cen} \gtrsim 5$ in an observational duration of $T_{\rm obs}$ = 4 yr in view of next-generation conceptual instruments. In particular, 4U 1543-62 b is a good target for DECIGO, while 2S 0918-549 b, 4U 0513-40 b, and 4U 1543-62 b are promising candidates for BBO.

For systems with a WD primary, eleven sources are identified as potential candidates, i.e., BW Scl b, CP Eri b, CR Boo b, EF Eri b, GP Com b, GW Lib b, SDSS J0926+3624 b, SDSS J1507+5230 b, SMSS J1606-1000 b, SRGeJ0453 b, and WZ Sge b. These sources yield a signal with $S/N_{\rm cen} \gtrsim 5$ in $T_{\rm obs}$ = 4 yr in view of such next-generation conceptual detectors as DECIGO and BBO. Among these sources, CR Boo b and WZ Sge b can even be detectable to some near-term GW observatories such as TianQin, LISA, and Taiji.

Planetary-mass objects around compact stars represent a promising class of targets for space-based GW instruments. However, they are unlikely to be detected by near-term detectors unless the systems have relatively large chirp masses and are close to us. Nevertheless, they are good targets for next-generation conceptual instruments. Especially, increasing the observation time and performing network observation by using more than one mission could significantly increase detectability. Gravitational wave observations of these systems can augment our comprehension of substellar mass objects near compact stars, which may include planets, brown dwarfs, or other objects with masses less than $80 M_{\rm Jup}$.

On the one hand, low-mass companions of compact stars could evolve into objects whose masses lie below 60 $M_{\rm Jup}$ (Sengar et al. 2017). Such binaries with a WD primary are thought to evolve into AM CVn systems through a series of evolutionary stages, yet their precise formation pathways remain obscure (Green et al. 2018; Chen et al. 2022). Systems with an NS primary can evolve into UCXBs, subsequently widening their orbits (Heinke et al. 2013; Chen et al. 2020). In such systems, NSs may eventually become millisecond radio PSRs, accompanied by planetary-mass objects (Wang et al. 2021a).

On the other hand, according to the strange quark matter hypothesis (Witten 1984), strange quark matter objects with masses ranging from planet to pulsar may exist, either in a bare state or covered by a crust of normal matter (Alcock et al. 1986; Kurban et al. 2022). The orbits of such planets can be remarkably tight, allowing them to venture extremely close to their host stars without being torn apart (Huang & Yu 2017; Kuerban et al. 2020).

The behavior and evolution of objects orbiting compact stars vary significantly, depending on their interior compositions. In strange-quark-matter planetary systems, tidal effects remain negligible until the final few inspiral orbits, provided the planet is fully bare (Wang et al. 2021b). Conversely, if the strange-matter core is covered by a normal-matter crust, the system may instead power electromagnetic transient phenomena (Geng et al. 2021; Zhou et al. 2025). In contrast, in binaries containing nondegenerate stars or tight systems with WDs, tidal interactions and mass loss can play crucial roles, resulting in discernible differences in the GW signal (Amaro-Seoane et al. 2023). The distinct signatures left in the GWs emitted by binary systems with planetary-mass companions around PSRs can provide valuable information on the composition of the secondary objects.

Investigating close-in planets around compact stars through GW astronomy offers a complementary avenue for discovering new ultrashort period planetary-mass companions. A multi-messenger approach, combining GW and electromagnetic observations, can provide deeper insights into the nature of these systems. Such joint analyses are expected to yield crucial information about both the formation and the long-term evolution of ultrashort-period planetary-mass companions orbiting compact stars, with valuable implications for physics and astrophysics.

Acknowledgements. We would like to thank the anonymous referee for helpful suggestions that led to a significant improvement of our work. This study is supported by the National Key R&D Program of China (Nos. 2022YFC2205202, 2021YFA0718500, 2022YFC2205203), the National Natural Science Foundation of China (Grant Nos. 12573051, 12288102, 12273028, 12233002, 12273100, 12303053), the Natural Science Foundation of Xinjiang Uygur Autonomous Region (Nos. 2022D01A363, 2023D01E20), the Major Science and Technology Program of Xinjiang Uygur Autonomous Region (No. 2022A03013-1), the Tianshan Talent Training Program of Xinjiang Uygur Autonomous Region, China (Grant Nos. 2023TSYCLJ0053, 2023TSYCTD0013), the Sichuan Provincial Natural Science Foundation Project (No. 2025ZNSFSC0878), the talent introduction program of Sichuan University of Science & Engineering (No. 2024RC15).

Y.F.H. acknowledges the support from the Xinjiang Tianchi Program. A.K. acknowledges the support from the Tianchi Talents Project of Xinjiang Uygur Autonomous Region. W.M.Y. is supported by the West Light Foundation of the Chinese Academy of Sciences (No. WLFC 2021-XBQNXZ027). Z.G.W. is supported by the 2021 project Xinjiang Uygur Autonomous Region of China for Tian Shan elites, the Youth Innovation Promotion Association of CAS under No. 2023069, and the Tianshan Talent Training Program (No. 2023TSYCCX0100).

References

Abbott, B. P., Abbott, R., Abbott, T. D., et al. 2016, Phys. Rev. Lett., 116, 061102
Abbott, B. P., Abbott, R., Abbott, T. D., et al. 2017, Phys. Rev. Lett., 119, 161101
Alcock, C., Farhi, E., & Olinto, A. 1986, ApJ, 310, 261
Amantayeva, A., Zharikov, S., Page, K. L., et al. 2021, ApJ, 918, 58
Amaro-Seoane, P., Audley, H., Babak, S., et al. 2017, arXiv e-prints [arXiv:1702.00786]
Amaro-Seoane, P., Andrews, J., Arca Sedda, M., et al. 2023, Liv. Rev. Relativ., 26, 2
Avakyan, A., Neumann, M., Zainab, A., et al. 2023, A&A, 675, A199
Bailer-Jones, C. A. L., Rybizki, J., Fouesneau, M., Mantelet, G., & Andrae, R. 2018, AJ, 156, 58
Baumgardt, H., & Vasiliev, E. 2021, MNRAS, 505, 5957
Breedt, E., Gänsicke, B. T., Marsh, T. R., et al. 2012, MNRAS, 425, 2548
Bult, P., Patruno, A., & van der Klis, M. 2015, ApJ, 814, 138
Burdge, K. B., Prince, T. A., Fuller, J., et al. 2020, ApJ, 905, 32
Burdge, K. B., Marsh, T. R., Fuller, J., et al. 2022, Nature, 605, 41
Carter, P. J., Steeghs, D., Marsh, T. R., et al. 2014, MNRAS, 437, 2894
Chen, M., & Liu, J. 2025, ApJ, 981, 175
Chen, W.-C., Liu, D.-D., & Wang, B. 2020, ApJ, 900, L8
Chen, H.-L., Chen, X., & Han, Z. 2022, ApJ, 935, 9
Chen, Z., Chen, Y., Chen, C., Ge, H., & Ma, B. 2024, A&A, 687, A256
Copperwheat, C. M., Marsh, T. R., Littlefair, S. P., et al. 2011, MNRAS, 410, 1113
Cunha, J. V., Silva, F. E., & Lima, J. A. S. 2018, MNRAS, 480, L28
Cunningham, T., Caiazzo, I., Sienkiewicz, G., et al. 2025, MNRAS, 540, 633
Cutler, C., & Harms, J. 2006, Phys. Rev. D, 73, 042001
Falanga, M., Bonnet-Bidaud, J. M., Poutanen, J., et al. 2005, A&A, 436, 647
Finn, L. S., & Thorne, K. S. 2000, Phys. Rev. D, 62, 124021
Fiore, W., Levin, L., McLaughlin, M. A., et al. 2023, ApJ, 956, 40
Gaia Collaboration (Brown, A. G. A., et al.) 2018, A&A, 616, A1
Gaia Collaboration (Vallenari, A., et al.) 2023, A&A, 674, A1
Galiullin, I., Rodriguez, A. C., Kulkarni, S. R., et al. 2024, MNRAS, 528, 676
Gençali, A. A., Niang, N., Toyran, O., et al. 2022, A&A, 658, A13
Geng, J. J., Huang, Y. F., & Lu, T. 2015, ApJ, 804, 21
Geng, J., Li, B., & Huang, Y. 2021, Innovation, 2, 100152
Gentile Fusillo, N. P., Tremblay, P.-E., Cukanovaite, E., et al. 2021, MNRAS, 508, 3877
Green, M. J., Marsh, T. R., Steeghs, D. T. H., et al. 2018, MNRAS, 476, 1663
Grieves, N., Bouchy, F., Lendl, M., et al. 2021, A&A, 652, A127
Groot, P. J., Nelemans, G., Steeghs, D., & Marsh, T. R. 2001, ApJ, 558, L123
Hamers, A. S. 2021, RNAAS, 5, 275
Harry, G. M., Fritschel, P., Shaddock, D. A., Folkner, W., & Phinney, E. S. 2006, Class. Quant. Grav., 23, 4887
Hatzes, A. P., & Rauer, H. 2015, ApJ, 810, L25
Heinke, C. O., Edmonds, P. D., & Grindlay, J. E. 2001, ApJ, 562, 363
Heinke, C. O., Ivanova, N., Engel, M. C., et al. 2013, ApJ, 768, 184
Hernández Santisteban, J. V., Knigge, C., Littlefair, S. P., et al. 2016, Nature, 533, 366
Homer, L., Charles, P. A., Naylor, T., et al. 1996, MNRAS, 282, L37
Huang, Y. F., & Yu, Y. B. 2017, ApJ, 848, 115
Huang, S.-J., Hu, Y.-M., Korol, V., et al. 2020, Phys. Rev. D, 102, 063021
İkis Gün, G., Karagül, A., & Gök, F. 2013, New A, 25, 1
In't Zand, J. J. M., Jonker, P. G., & Markwardt, C. B. 2007, A&A, 465, 953
Isogai, K., Kato, T., Monard, B., et al. 2019, PASJ, 71, 48
Jonker, P. G., & Nelemans, G. 2004, MNRAS, 354, 355
Kandel, D., & Romani, R. W. 2023, ApJ, 942, 6
Kawamura, S., Nakamura, T., Ando, M., et al. 2006, Class. Quant. Grav., 23, S125
Kawka, A., Vennes, S., Ferrario, L., et al. 2021, MNRAS, 507, L30
Keek, L., Iwakiri, W., Serino, M., et al. 2017, ApJ, 836, 111
Knigge, C. 2006, MNRAS, 373, 484
Kolbin, A. I., Fatkhullin, T. A., Pavlenko, E. P., et al. 2024, Astron. Lett., 50, 687
Kuerban, A., Geng, J.-J., & Huang, Y.-F. 2019, in American Institute of Physics Conference Series, 2127, Xiamen-CUSTIPEN Workshop on the Equation of State of Dense Neutron-Rich Matter in the Era of Gravitational Wave Astronomy, 020027
Kuerban, A., Geng, J.-J., Huang, Y.-F., Zong, H.-S., & Gong, H. 2020, ApJ, 890, 41
Kupfer, T., Steeghs, D., Groot, P. J., et al. 2016, MNRAS, 457, 1828
Kupfer, T., Korol, V., Shah, S., et al. 2018, MNRAS, 480, 302
Kupfer, T., Korol, V., Littenberg, T. B., et al. 2024, ApJ, 963, 100
Kurban, A., Huang, Y.-F., Geng, J.-J., & Zong, H.-S. 2022, Phys. Lett. B, 832, 137204
Levine, A., Ma, C. P., McClintock, J., et al. 1988, ApJ, 327, 732
Littlefair, S. P., Dhillon, V. S., Marsh, T. R., et al. 2006, Science, 314, 1578
Littlefair, S. P., Dhillon, V. S., Marsh, T. R., et al. 2007, MNRAS, 381, 827
Littlefair, S. P., Dhillon, V. S., Marsh, T. R., et al. 2008, MNRAS, 388, 1582
Liu, C., Ruan, W.-H., & Guo, Z.-K. 2023, Phys. Rev. D, 107, 064021
Luo, J., Chen, L.-S., Duan, H.-Z., et al. 2016, Class. Quant. Grav., 33, 035010
Ma, B., & Ge, J. 2014, MNRAS, 439, 2781
Markwardt, C. B., Swank, J. H., Strohmayer, T. E., in 't Zand, J. J. M., & Marshall, F. E. 2002, ApJ, 575, L21
McAllister, M. J., Littlefair, S. P., Dhillon, V. S., et al. 2017, MNRAS, 467, 1024
Mikhailov, K., van Leeuwen, J., & Jonker, P. G. 2017, ApJ, 840, 9
Moore, C. J., Cole, R. H., & Berry, C. P. L. 2015, Class. Quant. Grav., 32, 015014
Muñoz-Giraldo, D., Stelzer, B., & Schwope, A. 2024, A&A, 687, A305
Nather, R. E., Robinson, E. L., & Stover, R. J. 1981, ApJ, 244, 269
Neustroev, V. V., & Mäntynen, I. 2023, MNRAS, 523, 6114
Otulakowska-Hypka, M., Olech, A., de Miguel, E., et al. 2013, MNRAS, 429, 868
Pala, A. F., Schmidtobreick, L., Tappert, C., Gänsicke, B. T., & Mehner, A. 2018, MNRAS, 481, 2523
Pala, A. F., Gänsicke, B. T., Breedt, E., et al. 2020, MNRAS, 494, 3799
Pala, A. F., Gänsicke, B. T., Belloni, D., et al. 2022, MNRAS, 510, 6110
Papitto, A., Menna, M. T., Burderi, L., di Salvo, T., & Riggio, A. 2008, MNRAS, 383, 411
Parsons, S. G., Hermes, J. J., Marsh, T. R., et al. 2017, MNRAS, 471, 976
Peters, P. C., & Mathews, J. 1963, Phys. Rev., 131, 435
Prodan, S., & Murray, N. 2015, ApJ, 798, 117
Robson, T., Cornish, N. J., & Liu, C. 2019, Class. Quant. Grav., 36, 105011
Rodriguez, A. C., Galiullin, I., Gilfanov, M., et al. 2023, ApJ, 954, 63
Roelofs, G. H. A., Groot, P. J., Marsh, T. R., et al. 2005, MNRAS, 361, 487
Roelofs, G. H. A., Groot, P. J., Benedict, G. F., et al. 2007, ApJ, 666, 1174
Ruan, W.-H., Guo, Z.-K., Cai, R.-G., & Zhang, Y.-Z. 2020, Int. J. Mod. Phys. A, 35, 2050075
Sanna, A., Papitto, A., Burderi, L., et al. 2017, A&A, 598, A34
Schneider, J., Dedieu, C., Le Sidaner, P., Savalle, R., & Zolotukhin, I. 2011, A&A, 532, A79
Schwarz, G. J., Barman, T., Silvestri, N., et al. 2004, PASP, 116, 1111
Sengar, R., Tauris, T. M., Langer, N., & Istrate, A. G. 2017, MNRAS, 470, L6
Shahbaz, T., Watson, C. A., Zurita, C., Villaver, E., & Hernandez-Peralta, H. 2008, PASP, 120, 848
Southworth, J., Tappert, C., Gänsicke, B. T., & Copperwheat, C. M. 2015, A&A, 573, A61
Spiegel, D. S., Burrows, A., & Milsom, J. A. 2011, ApJ, 727, 57
Stovall, K., Lynch, R. S., Ransom, S. M., et al. 2014, ApJ, 791, 67
Strohmayer, T. E., Arzoumanian, Z., Bogdanov, S., et al. 2018, ApJ, 858, L13
Sun, M., & Li, J. 2023, arXiv e-prints [arXiv:2312.07834]
Sun, M., Li, J., Cao, S., & Liu, X. 2024, A&A, 682, A177
Suvorov, A. G. 2021, MNRAS, 503, 5495
van Roestel, J., Kupfer, T., Green, M. J., et al. 2022, MNRAS, 512, 5440
van Spaandonk, L., Steeghs, D., Marsh, T. R., & Parsons, S. G. 2010, ApJ, 715, L109
van Teeseling, A., Hessman, F. V., & Romani, R. W. 1999, A&A, 342, L45
Wagg, T., Breivik, K., & de Mink, S. E. 2022, ApJS, 260, 52
Wang, Z., & Chakrabarty, D. 2004, ApJ, 616, L139
Wang, B., Chen, W.-C., Liu, D.-D., et al. 2021a, MNRAS, 506, 4654
Wang, X., Kuerban, A., Geng, J.-J., et al. 2021b, Phys. Rev. D, 104, 123028
Wild, J. F., Littlefair, S. P., Ashley, R. P., et al. 2022, MNRAS, 509, 5086
Witten, E. 1984, Phys. Rev. D, 30, 272
Wong, K. W. K., Berti, E., Gabella, W. E., & Holley-Bockelmann, K. 2019, MNRAS, 483, L33
Wu, J., & Li, J. 2023, Phys. Rev. D, 108, 124047
Yagi, K., & Seto, N. 2011, Phys. Rev. D, 83, 044011
Yagi, K., & Seto, N. 2017, Phys. Rev. D, 95, 109901
Yu, S., Lu, Y., & Jeffery, C. S. 2021, MNRAS, 503, 2776
Zhang, X.-L., Huang, Y.-F., & Zou, Z.-C. 2024a, Front. Astron. Space Sci., 11, 1409463
Zhang, X.-L., Zou, Z.-C., Huang, Y.-F., et al. 2024b, MNRAS, 531, 3905
Zhong, J., & Wang, Z. 2011, ApJ, 729, 8
Zhou, X., Kurban, A., Liu, W.-T., Wang, N., & Yuan, Y.-J. 2025, ApJ, 986, 98
Zorotovic, M., & Schreiber, M. 2022, MNRAS, 513, 3587
Zurek, D. R., Knigge, C., Maccarone, T. J., Dieball, A., & Long, K. S. 2009, ApJ, 699, 1113

Appendix A: Observed and derived properties of the investigated sources

For the investigated sources, the parameters observed electromagnetically and the derivative of the GW frequency ($\dot{f}_{\rm gw}$) are presented in Table A.1, and the S/N values of the GW calculated for various detectors and observation durations are listed in Table A.2.

Table A.1: Parameters of the sources considered in this study.

Source name	m_2 ($M_{\rm jup}$)	$P_{\rm orb}$ (day)	e	D_L (pc)	m_1 ($M_\odot$)	$\dot{f}_{\rm gw}$ (Hz s^{-1})	References
Source with a PSR primary							
2S 0918-549 b	27.8±2.6	0.012083	...	4243^{+1468}_{-868}	1.4	2.08e-18	[1,2]
4U 0513-40 b	47.1	0.011806	...	11951^{+134}_{-133}	1.4	3.81e-18	[3,4,5]
4U 0614+09 b	14.9	0.035625	...	3300^{+1300}_{-2400}	1.4	2.12e-20	[4,6,7]
4U 1543-62 b	42.4	0.012500	...	3300^{+3300}_{-1900}	1.4	2.79e-18	[4,8,9]
4U 1626-67 b	41.9	0.027777	...	4500 ± 1500	1.4	1.47e-19	[4,10,11]
4U 1850-086 b	41.9	0.014292	...	7382^{+240}_{-233}	1.4	1.69e-18	[4,5,12]
4U 1905+000 b	52.4	0.055417	...	8750 ± 1250	1.4	1.46e-20	[4,13,14]
IGR J17062-6143 b	22.6	0.026368	...	7300 ± 500	1.7±0.3	1.10e-19	[4,15,16]
M15 X-2 b	35.6	0.015667	...	10709^{+96}_{-95}	1.4	1.02e-18	[4,17]
MAXI J0911-655 b	29.3	0.030764	...	10060^{+112}_{-111}	1.4	7.11e-20	[5,18]
NGC 6440 X-2 b	8.0	0.040022	0.07	8248^{+248}_{-241}	1.4	7.67e-21	[5,19]
NGC 6652B b	17.4	0.030278	...	9464^{+139}_{-137}	1.4	4.49e-20	[4,5,20]
PSR J0636+5129 b	8.5	0.066551	...	210^{+30}_{-20}	1.4	1.22e-21	[21,22]
PSR J1311-3430 b	12.6±0.6	0.065000	...	3010 ± 150	2.22±0.1	2.69e-21	[23]
PSR J1653-0158 b	14.7±1.0	0.052083	...	870^{+70}_{-80}	2.15±0.16	6.92e-21	[23]
XB 1916-053 b	15.6±1.0	0.034583	...	8800 ± 1300	1.4	2.47e-20	[4,14,24]
XTE J1751-305 b	36.7	0.029460	...	7600 ± 900	1.7±0.3	1.19e-19	[4,25,26]
XTE J1807-294 b	15.6±7.5	0.027829	...	5500 ± 2500	1.5±0.5	5.74e-20	[4,27]
ZTF J1406+1222 Ab	52.4	0.054057	...	1140 ± 200	1.4	1.60e-20	[28]
Source with a WD primary							
AL Com b	49.2±10.5	0.056668	...	523^{+252}_{-149}	0.9±0.3	9.37e-21	[29,30]
ASASSN-16kr b	44.0±1.0	0.061286	...	$160.50^{+7.16}_{-6.57}$	0.952±0.018	6.54e-21	[31,32]
ASASSN-17jf b	62.9±8.4	0.056790	...	$260.70^{+62.55}_{-42.27}$	0.669±0.031	9.63e-21	[2,31]
BW Scl b	53.4±6.3	0.054324	...	$93.65^{+0.46}_{-0.46}$	0.85±0.04	1.14e-20	[33]
CP Eri b	51.3±21.0	0.019690	...	$743.44^{+191.84}_{-126.54}$	0.8±0.1	4.34e-19	[2,34,35]
CR Boo b	69.1±23.0	0.017025	...	$351.64^{+4.60}_{-4.48}$	0.885±0.215	1.06e-18	[2,34,36]
CRTS J012059.6+325545 b	49.8±5.3	0.057145	...	$330.04^{+54.10}_{-40.74}$	0.586±0.29	6.84e-21	[2,37,38]
CRTS J1122-1110 b	14.7±5.2	0.045300	...	$701.16^{+930.69}_{-254.66}$	0.83±0.23	6.08e-21	[2,39]
DI UMa b	53.4±11.5	0.054558	...	685^{+43}_{-31}	0.83±0.17	1.10e-20	[30,40]
EF Eri b	83.7±3.0	0.056260	...	$160.44^{+3.73}_{-3.57}$	0.9	1.62e-20	[2,38]
EG Cnc b	32.5±7.3	0.059940	...	$186.55^{+7.21}_{-6.69}$	1.03±0.05	5.55e-21	[2,29,30]
EPIC 212235321 b	57.6±10.5	0.047370	...	$386.83^{+26.99}_{-23.68}$	0.47±0.01	1.35e-20	[32,41,42]
EZ Lyn b	44.0±14.7	0.059580	...	$142.78^{+2.29}_{-2.22}$	0.85±0.1	6.72e-21	[43]
GP Com b	26.2±16.6	0.032338	...	72.83 ± 0.24	0.528±0.027	2.74e-20	[2,44,45]
GW Lib b	52.4±7.3	0.053300	...	$113.05^{+0.79}_{-0.78}$	0.84±0.02	1.19e-20	[2,46]
IX Draconis b	58.1±26.6	0.064800	...	$752.11^{+23.27}_{-21.91}$	0.7±0.1	5.67e-21	[2,38,47]
NSV 1440 b	30.6	0.025233	...	$324.23^{+8.80}_{-8.35}$	0.65	9.14e-20	[2,48]
OGLE BLG-DN-7 b	51.3±12.4	0.059558	...	$176.51^{+3.11}_{-3.00}$	0.388±0.045	4.54e-21	[2,37,38]
OT J1112-3538 b	36.4±1.2	0.058500	...	$499.25^{+180.19}_{-104.65}$	0.338±0.286	3.16e-21	[2,37,38]
PQ And b	58.7	0.055800	...	$267.47^{+16.29}_{-14.53}$	0.47±0.13	7.51e-21	[2,38,49]
PR Her b	43.0	0.054200	...	$571.46^{+204.27}_{-119.12}$	0.34	4.93e-21	[2,37,38]

Table A.1: Continued.

Source name	m_2 ($M_{\rm jup}$)	$P_{\rm orb}$ (day)	e	D_L (pc)	m_1 ($M_\odot$)	$\dot{f}_{\rm gw}$ (Hz s^{-1})	References
QZ Lib b	33.5±12.6	0.064360	...	$187.36^{+12.43}_{-10.97}$	0.83±0.23	3.81e-21	[32,50]
SDSS J0926+3624 b	36.7±3.1	0.019650	...	$548.31^{+235.95}_{-126.81}$	0.85±0.04	3.28e-19	[32,51]
SDSS J1035+0551 b	54.5±2.1	0.057000	...	$195.24^{+11.57}_{-10.34}$	0.94±0.01	1.04e-20	[2,52,53]
SDSS J1057+2759 b	45.7±2.1	0.062800	...	$343.76^{+49.69}_{-38.55}$	0.8±0.015	5.51e-21	[2,54,55]
SDSS J1240-0159 b	32.5	0.025940	...	$658.02^{+290.47}_{-154.27}$	0.38	6.05e-20	[2,56]
SDSS J1339+4847 b	55.3	0.057290	...	$151.08^{+1.48}_{-1.45}$	0.42±0.02	5.95e-21	[2,37,38]
SDSS J1507+5230 b	58.7±1.1	0.046667	...	160 ± 10	0.9±0.01	2.27e-20	[57]
SDSS J1433+1011 b	57.6±8.4	0.054241	...	$233.29^{+8.85}_{-8.22}$	0.8±0.07	1.18e-20	[2,58]
SDSS J1730+5545 b	6.0	0.024444	...	$1232.44^{+573.59}_{-297.07}$	0.6	1.93e-20	[2,59]
SMSS J1606-1000 b	68.1±5.2	0.063915	...	$107.90^{+1.56}_{-1.52}$	0.72±0.05	7.10e-21	[2,38,60]
SRGeJ0411 b	41.9	0.067728	...	$320.10^{+30.01}_{-25.27}$	0.84±0.07	3.97e-21	[61,62]
SRGeJ0453 b	46.1±21.0	0.038250	...	$234.80^{+9.80}_{-9.05}$	0.85±0.04	3.57e-20	[32,62]
SSS J0522-3505 b	44.0±0.4	0.062193	...	$823.72^{+298.61}_{-173.11}$	0.76±0.023	5.32e-21	[31,62]
SW UMa b	60.8±11.5	0.056810	...	$161.29^{+1.58}_{-1.55}$	0.71±0.22	9.70e-21	[2,38,63]
V1108 Her b	47.2±9.7	0.056854	...	$147.98^{+2.22}_{-2.16}$	0.88±0.09	8.76e-21	[2,29,38]
V592 Her b	38.1±7.1	0.056097	...	710 ± 70	0.6	5.74e-21	[38,64]
WD 1202-024 b	51.3±6.3	0.049465	...	$664.98^{+124.16}_{-90.40}$	0.39±0.02	9.01e-21	[2,65]
WD J1820 b	41.9±31.4	0.065790	...	$212.62^{+24.00}_{-19.58}$	0.75±0.18	4.09e-21	[2,66]
WZ Sge b	60.1±9.3	0.056688	...	45.24 ± 0.06	0.85±0.04	1.10e-20	[2,30,38]
ZTF J0003+14 b	17.8±11.5	0.038540	...	$247.97^{+38.93}_{-29.63}$	0.79±0.11	1.29e-20	[2,67]
ZTF J0220+21 b	14.7±6.3	0.037150	...	$340.04^{+71.33}_{-50.25}$	0.83±0.07	1.26e-20	[2,67]
ZTF J0407-00 b	19.9±3.1	0.024583	...	$747.22^{+287.02}_{-162.32}$	0.79±0.06	7.49e-20	[2,67]
ZTF J1637+49 b	24.1±8.4	0.042710	...	$204.70^{+8.57}_{-7.91}$	0.9±0.05	1.30e-20	[2,67]
ZTF J2252-05 b	27.2±8.4	0.025970	...	$511.98^{+97.96}_{-70.85}$	0.76±0.05	8.14e-20	[2,67]
Gaia 19cwm b	76.5±15.7	0.059945	...	$237.39^{+14.08}_{-12.59}$	0.66±0.06	9.46e-21	[2,68]
Gaia14aae b	26.2±1.4	0.034510	...	$257.10^{+7.92}_{-7.46}$	0.87±0.02	3.03e-20	[2,67,69]

Notes. The secondary mass (m_2), orbital period ($P_{\rm orb}$), eccentricity (e), distance (D_L), and primary mass (m_1) are referenced from the published literature listed in the last column. The $\dot{f}_{\rm gw}$ is computed in this work.

References. [1] Zhong & Wang (2011); [2] Gaia Collaboration (2023); [3] Zurek et al. (2009); [4] Avakyan et al. (2023); [5] Baumgardt & Vasiliev (2021); [6] Yu et al. (2021); [7] Shahbaz et al. (2008); [8] Wang & Chakrabarty (2004); [9] Bailer-Jones et al. (2018); [10] Gençali et al. (2022); [11] Levine et al. (1988); [12] Homer et al. (1996); [13] Mikhailov et al. (2017); [14] Jonker & Nelemans (2004); [15] Strohmayer et al. (2018); [16] Keek et al. (2017); [17] Prodan & Murray (2015); [18] Sanna et al. (2017); [19] Bult et al. (2015); [20] Heinke et al. (2001); [21] Stovall et al. (2014); [22] Fiore et al. (2023); [23] Kandel & Romani (2023); [24] In't Zand et al. (2007); [25] Markwardt et al. (2002); [26] Papitto et al. (2008); [27] Falanga et al. (2005); [28] Burdge et al. (2022); [29] Pala et al. (2022); [30] Knigge (2006); [31] Wild et al. (2022); [32] Gaia Collaboration (2018); [33] Neustroev & Mäntynen (2023); [34] Kupfer et al. (2024); [35] Groot et al. (2001); [36] Roelofs et al. (2007); [37] Gentile Fusillo et al. (2021); [38] Muñoz-Giraldo et al. (2024); [39] Breedt et al. (2012); [40] Pala et al. (2020); [41] Zorotovic & Schreiber (2022); [42] Chen et al. (2024); [43] Amantayeva et al. (2021); [44] Kupfer et al. (2016); [45] Nather et al. (1981); [46] van Spaandonk et al. (2010); [47] Otulakowska-Hypka et al. (2013); [48] Isogai et al. (2019); [49] Schwarz et al. (2004); [50] Pala et al. (2018); [51] Copperwheat et al. (2011); [52] Littlefair et al. (2006); [53] Littlefair et al. (2008); [54] McAllister et al. (2017); [55] Southworth et al. (2015); [56] Roelofs et al. (2005); [57] Littlefair et al. (2007); [58] Hernández Santisteban et al. (2016); [59] Carter et al. (2014); [60] Kawka et al. (2021); [61] Galiullin et al. (2024); [62] Rodriguez et al. (2023); [63] İkis Gün et al. (2013); [64] van Teeseling et al. (1999); [65] Parsons et al. (2017); [66] Cunningham et al. (2025); [67] van Roestel et al. (2022); [68] Kolbin et al. (2024); [69] Green et al. (2018).

Table A.2: S/N values calculated for various detectors and observation durations.

Source	TianQin			LISA			Taiji			DECIGO			BBO		
	2 yr	4 yr	8 yr	2 yr	4 yr	8 yr	2 yr	4 yr	8 yr	2 yr	4 yr	8 yr	2 yr	4 yr	8 yr
Source with a PSR primary															
2S 0918-549 b	$0.57^{+0.22}_{-0.19}$	$0.83^{+0.31}_{-0.27}$	$1.20^{+0.45}_{-0.39}$	$0.74^{+0.28}_{-0.24}$	$2.91^{+1.09}_{-0.94}$	$4.11^{+1.55}_{-1.34}$	$1.13^{+0.43}_{-0.37}$	$2.28^{+0.86}_{-0.74}$	$3.23^{+1.21}_{-1.05}$	$2.56^{+0.96}_{-0.83}$	$4.89^{+1.84}_{-1.59}$	$7.99^{+3.01}_{-2.60}$	$4.83^{+1.82}_{-1.57}$	$8.68^{+3.26}_{-2.82}$	$13.60^{+5.12}_{-4.42}$
4U 0513-40 b	$0.36^{+0.00}_{-0.00}$	$0.53^{+0.01}_{-0.01}$	$0.76^{+0.01}_{-0.01}$	$0.47^{+0.01}_{-0.01}$	$1.90^{+0.02}_{-0.02}$	$2.69^{+0.03}_{-0.03}$	$0.73^{+0.01}_{-0.01}$	$1.49^{+0.02}_{-0.02}$	$2.11^{+0.02}_{-0.02}$	$1.71^{+0.02}_{-0.02}$	$3.19^{+0.04}_{-0.04}$	$5.14^{+0.06}_{-0.06}$	$3.19^{+0.04}_{-0.04}$	$5.59^{+0.06}_{-0.06}$	$8.66^{+0.10}_{-0.10}$
4U 0614+09 b	$0.02^{+0.06}_{-0.01}$	$0.03^{+0.09}_{-0.01}$	$0.05^{+0.13}_{-0.01}$	$0.05^{+0.13}_{-0.01}$	$0.08^{+0.21}_{-0.02}$	$0.11^{+0.30}_{-0.03}$	$0.06^{+0.16}_{-0.02}$	$0.09^{+0.24}_{-0.02}$	$0.12^{+0.33}_{-0.04}$	$0.11^{+0.31}_{-0.03}$	$0.16^{+0.43}_{-0.05}$	$0.23^{+0.61}_{-0.06}$	$0.13^{+0.35}_{-0.04}$	$0.19^{+0.50}_{-0.05}$	$0.27^{+0.71}_{-0.08}$
4U 1543-62 b	$1.02^{+1.39}_{-0.51}$	$1.48^{+2.01}_{-0.74}$	$2.13^{+2.90}_{-1.07}$	$1.30^{+1.77}_{-0.65}$	$4.99^{+6.77}_{-2.49}$	$7.05^{+9.57}_{-3.53}$	$1.98^{+2.69}_{-0.99}$	$3.93^{+5.34}_{-1.97}$	$5.56^{+7.55}_{-2.78}$	$4.21^{+5.72}_{-2.11}$	$8.43^{+11.44}_{-4.21}$	$14.06^{+19.09}_{-7.03}$	$8.07^{+10.96}_{-4.04}$	$15.18^{+20.60}_{-7.59}$	$24.24^{+32.90}_{-12.12}$
4U 1626-67 b	$0.09^{+0.05}_{-0.02}$	$0.13^{+0.07}_{-0.03}$	$0.19^{+0.09}_{-0.05}$	$0.17^{+0.08}_{-0.04}$	$0.29^{+0.14}_{-0.07}$	$0.41^{+0.20}_{-0.10}$	$0.21^{+0.10}_{-0.05}$	$0.31^{+0.15}_{-0.08}$	$0.43^{+0.22}_{-0.11}$	$0.39^{+0.20}_{-0.10}$	$0.56^{+0.28}_{-0.14}$	$0.79^{+0.39}_{-0.20}$	$0.44^{+0.22}_{-0.11}$	$0.62^{+0.31}_{-0.15}$	$0.88^{+0.44}_{-0.22}$
4U 1850-086 b	$0.32^{+0.01}_{-0.01}$	$0.46^{+0.01}_{-0.01}$	$0.66^{+0.02}_{-0.02}$	$0.40^{+0.01}_{-0.01}$	$1.31^{+0.04}_{-0.04}$	$1.86^{+0.06}_{-0.06}$	$0.59^{+0.02}_{-0.02}$	$1.09^{+0.04}_{-0.03}$	$1.54^{+0.05}_{-0.05}$	$0.89^{+0.03}_{-0.03}$	$2.11^{+0.07}_{-0.07}$	$3.96^{+0.13}_{-0.12}$	$1.66^{+0.05}_{-0.05}$	$4.03^{+0.13}_{-0.13}$	$7.20^{+0.23}_{-0.23}$
4U 1905+000 b	$0.01^{+0.00}_{-0.00}$	$0.01^{+0.00}_{-0.00}$	$0.02^{+0.00}_{-0.00}$	$0.02^{+0.00}_{-0.00}$	$0.04^{+0.01}_{-0.00}$	$0.05^{+0.01}_{-0.01}$	$0.03^{+0.00}_{-0.00}$	$0.04^{+0.01}_{-0.01}$	$0.06^{+0.01}_{-0.01}$	$0.06^{+0.01}_{-0.01}$	$0.08^{+0.01}_{-0.01}$	$0.11^{+0.02}_{-0.01}$	$0.07^{+0.01}_{-0.01}$	$0.10^{+0.02}_{-0.01}$	$0.15^{+0.02}_{-0.02}$
IGR J17062-6143 b	$0.04^{+0.01}_{-0.01}$	$0.06^{+0.01}_{-0.01}$	$0.08^{+0.02}_{-0.01}$	$0.07^{+0.01}_{-0.01}$	$0.12^{+0.03}_{-0.02}$	$0.18^{+0.04}_{-0.03}$	$0.09^{+0.02}_{-0.02}$	$0.13^{+0.03}_{-0.02}$	$0.19^{+0.04}_{-0.03}$	$0.17^{+0.03}_{-0.03}$	$0.24^{+0.05}_{-0.04}$	$0.33^{+0.07}_{-0.06}$	$0.18^{+0.04}_{-0.03}$	$0.26^{+0.05}_{-0.04}$	$0.37^{+0.07}_{-0.06}$
M15 X-2 b	$0.15^{+0.00}_{-0.00}$	$0.21^{+0.00}_{-0.00}$	$0.30^{+0.00}_{-0.00}$	$0.19^{+0.00}_{-0.00}$	$0.55^{+0.00}_{-0.00}$	$0.77^{+0.01}_{-0.01}$	$0.27^{+0.00}_{-0.00}$	$0.47^{+0.00}_{-0.00}$	$0.67^{+0.01}_{-0.01}$	$0.44^{+0.00}_{-0.00}$	$0.77^{+0.01}_{-0.01}$	$1.63^{+0.01}_{-0.01}$	$0.48^{+0.00}_{-0.00}$	$1.51^{+0.01}_{-0.01}$	$3.07^{+0.03}_{-0.03}$
MAXI J0911-655 b	$0.02^{+0.00}_{-0.00}$	$0.03^{+0.00}_{-0.00}$	$0.05^{+0.00}_{-0.00}$	$0.04^{+0.00}_{-0.00}$	$0.07^{+0.00}_{-0.00}$	$0.10^{+0.00}_{-0.00}$	$0.05^{+0.00}_{-0.00}$	$0.08^{+0.00}_{-0.00}$	$0.11^{+0.00}_{-0.00}$	$0.10^{+0.00}_{-0.00}$	$0.14^{+0.00}_{-0.00}$	$0.20^{+0.00}_{-0.00}$	$0.11^{+0.00}_{-0.00}$	$0.16^{+0.00}_{-0.00}$	$0.23^{+0.00}_{-0.00}$
NGC 6440 X-2 b	$0.00^{+0.00}_{-0.00}$	$0.01^{+0.00}_{-0.00}$	$0.01^{+0.00}_{-0.00}$	$0.01^{+0.00}_{-0.00}$	$0.01^{+0.00}_{-0.00}$	$0.02^{+0.00}_{-0.00}$	$0.01^{+0.00}_{-0.00}$	$0.01^{+0.00}_{-0.00}$	$0.02^{+0.00}_{-0.00}$	$0.02^{+0.00}_{-0.00}$	$0.03^{+0.00}_{-0.00}$	$0.04^{+0.00}_{-0.00}$	$0.02^{+0.00}_{-0.00}$	$0.03^{+0.00}_{-0.00}$	$0.05^{+0.00}_{-0.00}$
NGC 6652B b	$0.01^{+0.00}_{-0.00}$	$0.02^{+0.00}_{-0.00}$	$0.03^{+0.00}_{-0.00}$	$0.03^{+0.00}_{-0.00}$	$0.05^{+0.00}_{-0.00}$	$0.07^{+0.00}_{-0.00}$	$0.03^{+0.00}_{-0.00}$	$0.05^{+0.00}_{-0.00}$	$0.07^{+0.00}_{-0.00}$	$0.07^{+0.00}_{-0.00}$	$0.09^{+0.00}_{-0.00}$	$0.13^{+0.00}_{-0.00}$	$0.07^{+0.00}_{-0.00}$	$0.10^{+0.00}_{-0.00}$	$0.15^{+0.00}_{-0.00}$
PSR J0636+5129 b	$0.04^{+0.00}_{-0.00}$	$0.06^{+0.01}_{-0.01}$	$0.08^{+0.01}_{-0.01}$	$0.10^{+0.01}_{-0.01}$	$0.15^{+0.02}_{-0.02}$	$0.22^{+0.02}_{-0.03}$	$0.12^{+0.01}_{-0.02}$	$0.18^{+0.02}_{-0.02}$	$0.26^{+0.03}_{-0.03}$	$0.26^{+0.03}_{-0.03}$	$0.36^{+0.04}_{-0.05}$	$0.51^{+0.05}_{-0.06}$	$0.35^{+0.04}_{-0.04}$	$0.49^{+0.05}_{-0.06}$	$0.69^{+0.07}_{-0.09}$
PSR J1311-3430 b	$0.01^{+0.00}_{-0.00}$	$0.01^{+0.00}_{-0.00}$	$0.01^{+0.00}_{-0.00}$	$0.02^{+0.00}_{-0.00}$	$0.02^{+0.00}_{-0.00}$	$0.03^{+0.00}_{-0.00}$	$0.02^{+0.00}_{-0.00}$	$0.03^{+0.00}_{-0.00}$	$0.04^{+0.00}_{-0.00}$	$0.04^{+0.00}_{-0.00}$	$0.05^{+0.01}_{-0.01}$	$0.08^{+0.01}_{-0.01}$	$0.05^{+0.01}_{-0.01}$	$0.07^{+0.01}_{-0.01}$	$0.10^{+0.01}_{-0.01}$
PSR J1653-0158 b	$0.04^{+0.01}_{-0.01}$	$0.06^{+0.01}_{-0.01}$	$0.09^{+0.02}_{-0.01}$	$0.11^{+0.02}_{-0.02}$	$0.16^{+0.03}_{-0.02}$	$0.23^{+0.04}_{-0.03}$	$0.13^{+0.02}_{-0.02}$	$0.19^{+0.04}_{-0.03}$	$0.27^{+0.05}_{-0.04}$	$0.25^{+0.05}_{-0.04}$	$0.35^{+0.07}_{-0.05}$	$0.50^{+0.10}_{-0.08}$	$0.32^{+0.06}_{-0.05}$	$0.45^{+0.09}_{-0.07}$	$0.63^{+0.12}_{-0.10}$
XB 1916-053 b	$0.01^{+0.00}_{-0.00}$	$0.01^{+0.00}_{-0.00}$	$0.02^{+0.01}_{-0.00}$	$0.02^{+0.01}_{-0.00}$	$0.03^{+0.01}_{-0.01}$	$0.05^{+0.01}_{-0.01}$	$0.03^{+0.01}_{-0.00}$	$0.04^{+0.01}_{-0.01}$	$0.05^{+0.01}_{-0.01}$	$0.05^{+0.01}_{-0.01}$	$0.07^{+0.02}_{-0.01}$	$0.10^{+0.02}_{-0.02}$	$0.06^{+0.01}_{-0.01}$	$0.08^{+0.02}_{-0.01}$	$0.11^{+0.03}_{-0.02}$
XTE J1751-305 b	$0.05^{+0.01}_{-0.01}$	$0.07^{+0.02}_{-0.01}$	$0.10^{+0.03}_{-0.02}$	$0.09^{+0.02}_{-0.02}$	$0.15^{+0.04}_{-0.03}$	$0.21^{+0.06}_{-0.04}$	$0.11^{+0.03}_{-0.02}$	$0.16^{+0.04}_{-0.03}$	$0.23^{+0.06}_{-0.05}$	$0.21^{+0.06}_{-0.04}$	$0.29^{+0.08}_{-0.06}$	$0.41^{+0.11}_{-0.09}$	$0.23^{+0.06}_{-0.05}$	$0.33^{+0.09}_{-0.07}$	$0.46^{+0.13}_{-0.10}$
XTE J1807-294 b	$0.03^{+0.06}_{-0.02}$	$0.04^{+0.08}_{-0.03}$	$0.06^{+0.11}_{-0.04}$	$0.05^{+0.10}_{-0.03}$	$0.09^{+0.18}_{-0.06}$	$0.13^{+0.25}_{-0.08}$	$0.07^{+0.13}_{-0.04}$	$0.10^{+0.19}_{-0.06}$	$0.14^{+0.26}_{-0.09}$	$0.13^{+0.24}_{-0.08}$	$0.18^{+0.34}_{-0.11}$	$0.25^{+0.48}_{-0.16}$	$0.14^{+0.27}_{-0.09}$	$0.20^{+0.38}_{-0.13}$	$0.28^{+0.53}_{-0.18}$
ZTF J1406+1222 Ab	$0.08^{+0.02}_{-0.01}$	$0.11^{+0.02}_{-0.02}$	$0.16^{+0.03}_{-0.02}$	$0.20^{+0.04}_{-0.03}$	$0.29^{+0.06}_{-0.04}$	$0.42^{+0.09}_{-0.06}$	$0.23^{+0.05}_{-0.03}$	$0.35^{+0.07}_{-0.05}$	$0.49^{+0.10}_{-0.07}$	$0.46^{+0.10}_{-0.07}$	$0.66^{+0.14}_{-0.10}$	$0.93^{+0.20}_{-0.14}$	$0.59^{+0.13}_{-0.09}$	$0.84^{+0.18}_{-0.13}$	$1.19^{+0.25}_{-0.18}$
Source with a WD primary															
AL Com b	$0.11^{+0.09}_{-0.05}$	$0.15^{+0.13}_{-0.08}$	$0.21^{+0.18}_{-0.11}$	$0.27^{+0.23}_{-0.14}$	$0.40^{+0.34}_{-0.21}$	$0.56^{+0.48}_{-0.29}$	$0.32^{+0.27}_{-0.16}$	$0.47^{+0.40}_{-0.24}$	$0.66^{+0.57}_{-0.35}$	$0.63^{+0.54}_{-0.33}$	$0.90^{+0.77}_{-0.47}$	$1.27^{+1.09}_{-0.66}$	$0.82^{+0.70}_{-0.43}$	$1.16^{+0.99}_{-0.60}$	$1.64^{+1.40}_{-0.85}$
ASASSN-16kr b	$0.26^{+0.02}_{-0.02}$	$0.36^{+0.03}_{-0.02}$	$0.52^{+0.04}_{-0.04}$	$0.67^{+0.05}_{-0.05}$	$0.98^{+0.07}_{-0.07}$	$1.39^{+0.10}_{-0.09}$	$0.79^{+0.06}_{-0.05}$	$1.17^{+0.08}_{-0.08}$	$1.65^{+0.12}_{-0.11}$	$1.61^{+0.11}_{-0.11}$	$2.27^{+0.16}_{-0.15}$	$3.21^{+0.23}_{-0.22}$	$2.12^{+0.15}_{-0.14}$	$3.00^{+0.21}_{-0.20}$	$4.24^{+0.30}_{-0.29}$
ASASSN-17jf b	$0.22^{+0.08}_{-0.06}$	$0.31^{+0.11}_{-0.09}$	$0.44^{+0.16}_{-0.13}$	$0.55^{+0.20}_{-0.17}$	$0.82^{+0.29}_{-0.24}$	$1.16^{+0.41}_{-0.35}$	$0.65^{+0.23}_{-0.19}$	$0.97^{+0.35}_{-0.29}$	$1.37^{+0.49}_{-0.41}$	$1.31^{+0.47}_{-0.39}$	$1.85^{+0.66}_{-0.55}$	$2.62^{+0.94}_{-0.78}$	$1.69^{+0.61}_{-0.51}$	$2.40^{+0.86}_{-0.72}$	$3.39^{+1.21}_{-1.01}$
BW Scl b	$0.68^{+0.09}_{-0.08}$	$0.97^{+0.12}_{-0.12}$	$1.38^{+0.18}_{-0.17}$	$1.73^{+0.22}_{-0.21}$	$2.56^{+0.33}_{-0.31}$	$3.62^{+0.46}_{-0.44}$	$2.04^{+0.26}_{-0.25}$	$3.03^{+0.39}_{-0.37}$	$4.29^{+0.55}_{-0.52}$	$4.06^{+0.52}_{-0.49}$	$5.74^{+0.74}_{-0.70}$	$8.12^{+1.04}_{-0.98}$	$5.19^{+0.67}_{-0.63}$	$7.34^{+0.94}_{-0.89}$	$10.38^{+1.33}_{-1.26}$
CP Eri b	$1.17^{+0.86}_{-0.59}$	$1.65^{+1.22}_{-0.83}$	$2.34^{+1.73}_{-1.18}$	$1.66^{+1.23}_{-0.84}$	$3.64^{+2.69}_{-1.83}$	$5.14^{+3.80}_{-2.59}$	$2.19^{+1.62}_{-1.10}$	$3.49^{+2.58}_{-1.76}$	$4.93^{+3.65}_{-2.48}$	$3.96^{+2.93}_{-2.00}$	$5.60^{+4.14}_{-2.82}$	$7.92^{+5.86}_{-3.99}$	$4.23^{+3.13}_{-2.13}$	$5.98^{+4.42}_{-3.01}$	$14.77^{+10.92}_{-7.44}$
CR Boo b	$5.14^{+2.11}_{-1.79}$	$7.31^{+3.00}_{-2.54}$	$10.41^{+4.27}_{-3.62}$	$6.79^{+2.79}_{-2.36}$	$17.55^{+7.20}_{-6.09}$	$24.82^{+10.19}_{-8.62}$	$9.34^{+3.83}_{-3.24}$	$15.82^{+6.49}_{-5.49}$	$22.37^{+9.18}_{-7.77}$	$15.97^{+6.56}_{-5.55}$	$22.59^{+9.27}_{-7.84}$	$48.70^{+19.99}_{-16.91}$	$16.83^{+6.91}_{-5.84}$	$39.48^{+16.20}_{-13.71}$	$94.34^{+38.72}_{-32.76}$
CRTS J012059.6+325545 b	$0.12^{+0.07}_{-0.05}$	$0.17^{+0.10}_{-0.07}$	$0.25^{+0.14}_{-0.11}$	$0.31^{+0.18}_{-0.13}$	$0.46^{+0.27}_{-0.20}$	$0.65^{+0.38}_{-0.28}$	$0.37^{+0.21}_{-0.16}$	$0.55^{+0.32}_{-0.23}$	$0.77^{+0.45}_{-0.33}$	$0.74^{+0.43}_{-0.32}$	$1.05^{+0.61}_{-0.45}$	$1.48^{+0.86}_{-0.63}$	$0.96^{+0.56}_{-0.41}$	$1.36^{+0.79}_{-0.58}$	$1.92^{+1.11}_{-0.82}$
CRTS J1122-1110 b	$0.04^{+0.05}_{-0.03}$	$0.06^{+0.07}_{-0.04}$	$0.08^{+0.10}_{-0.06}$	$0.10^{+0.12}_{-0.07}$	$0.15^{+0.18}_{-0.11}$	$0.21^{+0.26}_{-0.15}$	$0.12^{+0.14}_{-0.08}$	$0.17^{+0.21}_{-0.12}$	$0.24^{+0.30}_{-0.18}$	$0.22^{+0.28}_{-0.16}$	$0.31^{+0.39}_{-0.23}$	$0.45^{+0.56}_{-0.32}$	$0.27^{+0.34}_{-0.20}$	$0.38^{+0.48}_{-0.28}$	$0.54^{+0.68}_{-0.40}$
DI UMa b	$0.09^{+0.03}_{-0.03}$	$0.13^{+0.04}_{-0.04}$	$0.18^{+0.06}_{-0.05}$	$0.23^{+0.08}_{-0.07}$	$0.34^{+0.11}_{-0.10}$	$0.48^{+0.16}_{-0.14}$	$0.27^{+0.09}_{-0.08}$	$0.40^{+0.13}_{-0.12}$	$0.57^{+0.19}_{-0.16}$	$0.54^{+0.18}_{-0.15}$	$0.76^{+0.25}_{-0.22}$	$1.08^{+0.35}_{-0.31}$	$0.69^{+0.23}_{-0.20}$	$0.98^{+0.32}_{-0.28}$	$1.38^{+0.45}_{-0.40}$
EF Eri b	$0.59^{+0.03}_{-0.03}$	$0.83^{+0.05}_{-0.05}$	$1.18^{+0.07}_{-0.07}$	$1.49^{+0.09}_{-0.09}$	$2.21^{+0.13}_{-0.13}$	$3.13^{+0.18}_{-0.18}$	$1.76^{+0.10}_{-0.10}$	$2.62^{+0.15}_{-0.15}$	$3.70^{+0.22}_{-0.21}$	$3.53^{+0.21}_{-0.20}$	$4.99^{+0.30}_{-0.28}$	$7.06^{+0.42}_{-0.40}$	$4.56^{+0.27}_{-0.26}$	$6.44^{+0.38}_{-0.37}$	$9.11^{+0.54}_{-0.52}$
EG Cnc b	$0.18^{+0.05}_{-0.05}$	$0.26^{+0.07}_{-0.06}$	$0.37^{+0.10}_{-0.09}$	$0.48^{+0.13}_{-0.12}$	$0.70^{+0.20}_{-0.17}$	$0.99^{+0.28}_{-0.24}$	$0.56^{+0.16}_{-0.14}$	$0.83^{+0.23}_{-0.20}$	$1.17^{+0.33}_{-0.29}$	$1.14^{+0.32}_{-0.28}$	$1.61^{+0.45}_{-0.39}$	$2.27^{+0.64}_{-0.56}$	$1.49^{+0.42}_{-0.37}$	$2.11^{+0.59}_{-0.52}$	$2.98^{+0.84}_{-0.73}$
EPIC 212235321 b	$0.17^{+0.04}_{-0.04}$	$0.24^{+0.06}_{-0.05}$	$0.34^{+0.09}_{-0.08}$	$0.41^{+0.11}_{-0.09}$	$0.62^{+0.16}_{-0.14}$	$0.88^{+0.23}_{-0.20}$	$0.49^{+0.13}_{-0.11}$	$0.73^{+0.19}_{-0.16}$	$1.03^{+0.27}_{-0.23}$	$0.95^{+0.25}_{-0.21}$	$1.35^{+0.35}_{-0.30}$	$1.91^{+0.49}_{-0.43}$	$1.18^{+0.31}_{-0.26}$	$1.66^{+0.43}_{-0.37}$	$2.35^{+0.61}_{-0.53}$
EZ Lyn b	$0.29^{+0.11}_{-0.09}$	$0.41^{+0.16}_{-0.13}$	$0.58^{+0.22}_{-0.19}$	$0.75^{+0.29}_{-0.24}$	$1.10^{+0.42}_{-0.36}$	$1.55^{+0.59}_{-0.51}$	$0.88^{+0.33}_{-0.29}$	$1.30^{+0.50}_{-0.42}$	$1.84^{+0.70}_{-0.60}$	$1.78^{+0.68}_{-0.58}$	$2.52^{+0.96}_{-0.82}$	$3.57^{+1.36}_{-1.16}$	$2.34^{+0.89}_{-0.76}$	$3.30^{+1.26}_{-1.07}$	$4.67^{+1.78}_{-1.52}$

Table A.2: Continued.

Source	TianQin			LISA			Taiji			DECIGO			BBO		
	2 yr	4 yr	8 yr	2 yr	4 yr	8 yr	2 yr	4 yr	8 yr	2 yr	4 yr	8 yr	2 yr	4 yr	8 yr
GP Com b	$1.26^{+0.88}_{-0.68}$	$1.79^{+1.26}_{-0.97}$	$2.52^{+1.77}_{-1.37}$	$2.46^{+1.73}_{-1.34}$	$4.03^{+2.83}_{-2.19}$	$5.70^{+4.01}_{-3.10}$	$3.06^{+2.15}_{-1.66}$	$4.45^{+3.13}_{-2.42}$	$6.29^{+4.43}_{-3.42}$	$5.76^{+4.06}_{-3.13}$	$8.15^{+5.74}_{-4.43}$	$11.52^{+8.11}_{-6.26}$	$6.57^{+4.63}_{-3.57}$	$9.30^{+6.54}_{-5.05}$	$13.15^{+9.25}_{-7.14}$
GW Lib b	$0.58^{+0.09}_{-0.08}$	$0.82^{+0.12}_{-0.12}$	$1.17^{+0.18}_{-0.16}$	$1.46^{+0.22}_{-0.20}$	$2.17^{+0.32}_{-0.30}$	$3.06^{+0.46}_{-0.43}$	$1.72^{+0.26}_{-0.24}$	$2.56^{+0.38}_{-0.36}$	$3.62^{+0.54}_{-0.51}$	$3.42^{+0.51}_{-0.48}$	$4.83^{+0.72}_{-0.68}$	$6.83^{+1.02}_{-0.96}$	$4.34^{+0.65}_{-0.61}$	$6.14^{+0.92}_{-0.86}$	$8.69^{+1.30}_{-1.22}$
IX Draconis b	$0.05^{+0.03}_{-0.02}$	$0.07^{+0.04}_{-0.03}$	$0.10^{+0.05}_{-0.04}$	$0.13^{+0.07}_{-0.06}$	$0.19^{+0.10}_{-0.08}$	$0.27^{+0.15}_{-0.12}$	$0.15^{+0.08}_{-0.07}$	$0.23^{+0.12}_{-0.10}$	$0.32^{+0.18}_{-0.14}$	$0.32^{+0.17}_{-0.14}$	$0.45^{+0.25}_{-0.20}$	$0.64^{+0.35}_{-0.28}$	$0.43^{+0.23}_{-0.19}$	$0.61^{+0.33}_{-0.26}$	$0.86^{+0.47}_{-0.37}$
NSV 1440 b	$0.73^{+0.02}_{-0.02}$	$1.04^{+0.03}_{-0.03}$	$1.46^{+0.04}_{-0.04}$	$1.22^{+0.03}_{-0.03}$	$2.21^{+0.06}_{-0.06}$	$3.13^{+0.08}_{-0.08}$	$1.55^{+0.04}_{-0.04}$	$2.30^{+0.06}_{-0.06}$	$3.25^{+0.09}_{-0.09}$	$2.90^{+0.08}_{-0.08}$	$4.10^{+0.11}_{-0.11}$	$5.79^{+0.15}_{-0.15}$	$3.18^{+0.08}_{-0.08}$	$4.50^{+0.12}_{-0.12}$	$6.36^{+0.17}_{-0.17}$
OGLE BLG-DN-7 b	$0.16^{+0.04}_{-0.04}$	$0.22^{+0.06}_{-0.06}$	$0.32^{+0.09}_{-0.08}$	$0.41^{+0.11}_{-0.10}$	$0.60^{+0.17}_{-0.15}$	$0.85^{+0.24}_{-0.21}$	$0.48^{+0.13}_{-0.12}$	$0.71^{+0.20}_{-0.18}$	$1.01^{+0.28}_{-0.25}$	$0.97^{+0.27}_{-0.24}$	$1.38^{+0.39}_{-0.34}$	$1.95^{+0.55}_{-0.48}$	$1.28^{+0.36}_{-0.32}$	$1.81^{+0.51}_{-0.45}$	$2.55^{+0.72}_{-0.63}$
OT J1112-3538 b	$0.04^{+0.04}_{-0.02}$	$0.05^{+0.06}_{-0.04}$	$0.08^{+0.08}_{-0.05}$	$0.10^{+0.11}_{-0.06}$	$0.15^{+0.16}_{-0.09}$	$0.21^{+0.23}_{-0.13}$	$0.12^{+0.13}_{-0.07}$	$0.17^{+0.19}_{-0.11}$	$0.24^{+0.27}_{-0.16}$	$0.23^{+0.26}_{-0.15}$	$0.33^{+0.36}_{-0.21}$	$0.47^{+0.51}_{-0.30}$	$0.31^{+0.34}_{-0.20}$	$0.43^{+0.47}_{-0.28}$	$0.61^{+0.67}_{-0.39}$
PQ And b	$0.16^{+0.04}_{-0.04}$	$0.23^{+0.06}_{-0.05}$	$0.33^{+0.09}_{-0.08}$	$0.41^{+0.11}_{-0.10}$	$0.61^{+0.17}_{-0.14}$	$0.86^{+0.23}_{-0.20}$	$0.48^{+0.13}_{-0.11}$	$0.72^{+0.20}_{-0.17}$	$1.02^{+0.28}_{-0.24}$	$0.97^{+0.26}_{-0.23}$	$1.37^{+0.37}_{-0.32}$	$1.94^{+0.53}_{-0.45}$	$1.25^{+0.34}_{-0.29}$	$1.77^{+0.48}_{-0.41}$	$2.50^{+0.68}_{-0.58}$
PR Her b	$0.05^{+0.01}_{-0.01}$	$0.07^{+0.02}_{-0.02}$	$0.10^{+0.03}_{-0.03}$	$0.12^{+0.03}_{-0.03}$	$0.18^{+0.05}_{-0.05}$	$0.26^{+0.07}_{-0.07}$	$0.14^{+0.04}_{-0.04}$	$0.21^{+0.06}_{-0.06}$	$0.30^{+0.08}_{-0.08}$	$0.29^{+0.08}_{-0.08}$	$0.41^{+0.11}_{-0.11}$	$0.57^{+0.15}_{-0.15}$	$0.37^{+0.10}_{-0.10}$	$0.52^{+0.14}_{-0.14}$	$0.73^{+0.19}_{-0.19}$
QZ Lib b	$0.14^{+0.07}_{-0.06}$	$0.19^{+0.10}_{-0.08}$	$0.27^{+0.15}_{-0.11}$	$0.35^{+0.19}_{-0.15}$	$0.52^{+0.28}_{-0.22}$	$0.73^{+0.39}_{-0.31}$	$0.41^{+0.22}_{-0.17}$	$0.61^{+0.33}_{-0.26}$	$0.87^{+0.47}_{-0.36}$	$0.86^{+0.46}_{-0.36}$	$1.21^{+0.65}_{-0.51}$	$1.71^{+0.92}_{-0.72}$	$1.15^{+0.62}_{-0.48}$	$1.62^{+0.87}_{-0.68}$	$2.29^{+1.24}_{-0.96}$
SDSS J0926+3624 b	$1.19^{+0.50}_{-0.43}$	$1.68^{+0.71}_{-0.61}$	$2.39^{+1.00}_{-0.87}$	$1.69^{+0.71}_{-0.61}$	$3.72^{+1.56}_{-1.35}$	$5.26^{+2.21}_{-1.91}$	$2.24^{+0.94}_{-0.81}$	$3.56^{+1.50}_{-1.29}$	$5.03^{+2.12}_{-1.83}$	$4.04^{+1.70}_{-1.47}$	$5.71^{+2.40}_{-2.07}$	$8.08^{+3.40}_{-2.93}$	$4.31^{+1.81}_{-1.56}$	$6.09^{+2.56}_{-2.21}$	$15.18^{+6.39}_{-5.51}$
SDSS J1035+0551 b	$0.32^{+0.03}_{-0.03}$	$0.45^{+0.04}_{-0.04}$	$0.64^{+0.06}_{-0.06}$	$0.81^{+0.08}_{-0.07}$	$1.19^{+0.12}_{-0.11}$	$1.68^{+0.16}_{-0.15}$	$0.95^{+0.09}_{-0.09}$	$1.41^{+0.14}_{-0.13}$	$1.99^{+0.19}_{-0.18}$	$1.91^{+0.18}_{-0.18}$	$2.70^{+0.26}_{-0.25}$	$3.81^{+0.37}_{-0.35}$	$2.47^{+0.24}_{-0.23}$	$3.49^{+0.34}_{-0.32}$	$4.94^{+0.48}_{-0.45}$
SDSS J1057+2759 b	$0.10^{+0.02}_{-0.02}$	$0.15^{+0.03}_{-0.02}$	$0.21^{+0.04}_{-0.03}$	$0.27^{+0.05}_{-0.05}$	$0.40^{+0.07}_{-0.07}$	$0.56^{+0.10}_{-0.09}$	$0.32^{+0.06}_{-0.05}$	$0.47^{+0.08}_{-0.08}$	$0.67^{+0.12}_{-0.11}$	$0.65^{+0.12}_{-0.11}$	$0.92^{+0.17}_{-0.15}$	$1.31^{+0.23}_{-0.22}$	$0.87^{+0.16}_{-0.14}$	$1.23^{+0.22}_{-0.20}$	$1.74^{+0.31}_{-0.29}$
SDSS J1240-0159 b	$0.25^{+0.08}_{-0.08}$	$0.35^{+0.11}_{-0.11}$	$0.49^{+0.15}_{-0.15}$	$0.42^{+0.13}_{-0.13}$	$0.75^{+0.23}_{-0.23}$	$1.05^{+0.32}_{-0.32}$	$0.53^{+0.16}_{-0.16}$	$0.78^{+0.24}_{-0.24}$	$1.10^{+0.34}_{-0.34}$	$0.99^{+0.30}_{-0.30}$	$1.40^{+0.43}_{-0.43}$	$1.98^{+0.61}_{-0.61}$	$1.09^{+0.33}_{-0.33}$	$1.54^{+0.47}_{-0.47}$	$2.18^{+0.67}_{-0.67}$
SDSS J1339+4847 b	$0.23^{+0.01}_{-0.01}$	$0.33^{+0.01}_{-0.01}$	$0.47^{+0.02}_{-0.02}$	$0.60^{+0.03}_{-0.03}$	$0.88^{+0.04}_{-0.04}$	$1.25^{+0.05}_{-0.05}$	$0.70^{+0.03}_{-0.03}$	$1.04^{+0.05}_{-0.04}$	$1.48^{+0.06}_{-0.06}$	$1.42^{+0.06}_{-0.06}$	$2.00^{+0.09}_{-0.09}$	$2.83^{+0.12}_{-0.12}$	$1.83^{+0.08}_{-0.08}$	$2.59^{+0.11}_{-0.11}$	$3.67^{+0.16}_{-0.16}$
SDSS J1507+5230 b	$0.68^{+0.06}_{-0.05}$	$0.98^{+0.09}_{-0.08}$	$1.38^{+0.12}_{-0.11}$	$1.64^{+0.14}_{-0.13}$	$2.48^{+0.22}_{-0.19}$	$3.50^{+0.31}_{-0.27}$	$1.96^{+0.17}_{-0.15}$	$2.90^{+0.26}_{-0.22}$	$4.10^{+0.36}_{-0.32}$	$3.80^{+0.33}_{-0.29}$	$5.38^{+0.47}_{-0.42}$	$7.61^{+0.67}_{-0.59}$	$4.68^{+0.41}_{-0.36}$	$6.62^{+0.58}_{-0.51}$	$9.36^{+0.82}_{-0.73}$
SDSS J1433+1011 b	$0.28^{+0.06}_{-0.05}$	$0.40^{+0.08}_{-0.07}$	$0.57^{+0.12}_{-0.10}$	$0.72^{+0.15}_{-0.13}$	$1.07^{+0.22}_{-0.19}$	$1.51^{+0.30}_{-0.27}$	$0.85^{+0.17}_{-0.15}$	$1.26^{+0.25}_{-0.23}$	$1.78^{+0.36}_{-0.32}$	$1.69^{+0.34}_{-0.31}$	$2.39^{+0.48}_{-0.43}$	$3.38^{+0.68}_{-0.61}$	$2.16^{+0.44}_{-0.39}$	$3.05^{+0.62}_{-0.55}$	$4.31^{+0.87}_{-0.78}$
SDSS J1730+5545 b	$0.04^{+0.01}_{-0.01}$	$0.06^{+0.02}_{-0.02}$	$0.08^{+0.02}_{-0.02}$	$0.06^{+0.02}_{-0.02}$	$0.12^{+0.04}_{-0.04}$	$0.17^{+0.05}_{-0.05}$	$0.08^{+0.03}_{-0.03}$	$0.12^{+0.04}_{-0.04}$	$0.17^{+0.05}_{-0.05}$	$0.15^{+0.05}_{-0.05}$	$0.22^{+0.07}_{-0.07}$	$0.30^{+0.10}_{-0.10}$	$0.17^{+0.05}_{-0.05}$	$0.24^{+0.07}_{-0.07}$	$0.33^{+0.11}_{-0.11}$
SMSS J1606-1000 b	$0.43^{+0.05}_{-0.04}$	$0.61^{+0.06}_{-0.06}$	$0.87^{+0.09}_{-0.09}$	$1.13^{+0.12}_{-0.11}$	$1.66^{+0.18}_{-0.17}$	$2.34^{+0.25}_{-0.24}$	$1.33^{+0.14}_{-0.13}$	$1.97^{+0.21}_{-0.20}$	$2.78^{+0.30}_{-0.28}$	$2.75^{+0.29}_{-0.28}$	$3.89^{+0.41}_{-0.39}$	$5.49^{+0.58}_{-0.55}$	$3.67^{+0.39}_{-0.37}$	$5.19^{+0.55}_{-0.52}$	$7.34^{+0.78}_{-0.74}$
SRGeJ0411 b	$0.09^{+0.01}_{-0.01}$	$0.12^{+0.02}_{-0.02}$	$0.17^{+0.03}_{-0.02}$	$0.23^{+0.03}_{-0.03}$	$0.33^{+0.05}_{-0.05}$	$0.47^{+0.07}_{-0.06}$	$0.27^{+0.04}_{-0.04}$	$0.39^{+0.06}_{-0.05}$	$0.56^{+0.08}_{-0.08}$	$0.56^{+0.08}_{-0.08}$	$0.79^{+0.12}_{-0.11}$	$1.12^{+0.17}_{-0.15}$	$0.76^{+0.11}_{-0.10}$	$1.07^{+0.16}_{-0.15}$	$1.52^{+0.22}_{-0.21}$
SRGeJ0453 b	$0.60^{+0.33}_{-0.26}$	$0.86^{+0.47}_{-0.37}$	$1.21^{+0.66}_{-0.52}$	$1.30^{+0.71}_{-0.56}$	$2.04^{+1.12}_{-0.88}$	$2.89^{+1.58}_{-1.24}$	$1.60^{+0.87}_{-0.69}$	$2.33^{+1.27}_{-1.00}$	$3.30^{+1.80}_{-1.42}$	$3.03^{+1.66}_{-1.30}$	$4.28^{+2.34}_{-1.84}$	$6.05^{+3.31}_{-2.61}$	$3.56^{+1.95}_{-1.53}$	$5.04^{+2.76}_{-2.17}$	$7.13^{+3.90}_{-3.07}$
SSS J0522-3505 b	$0.04^{+0.01}_{-0.01}$	$0.06^{+0.02}_{-0.02}$	$0.08^{+0.02}_{-0.02}$	$0.11^{+0.03}_{-0.03}$	$0.16^{+0.05}_{-0.04}$	$0.22^{+0.07}_{-0.06}$	$0.13^{+0.04}_{-0.04}$	$0.19^{+0.06}_{-0.05}$	$0.27^{+0.08}_{-0.07}$	$0.26^{+0.08}_{-0.07}$	$0.37^{+0.11}_{-0.10}$	$0.52^{+0.15}_{-0.15}$	$0.34^{+0.10}_{-0.10}$	$0.49^{+0.14}_{-0.14}$	$0.69^{+0.20}_{-0.19}$
SW UMa b	$0.35^{+0.11}_{-0.10}$	$0.50^{+0.16}_{-0.14}$	$0.71^{+0.22}_{-0.20}$	$0.90^{+0.28}_{-0.25}$	$1.33^{+0.42}_{-0.36}$	$1.88^{+0.59}_{-0.52}$	$1.06^{+0.33}_{-0.29}$	$1.58^{+0.49}_{-0.43}$	$2.23^{+0.70}_{-0.61}$	$2.13^{+0.66}_{-0.58}$	$3.02^{+0.94}_{-0.83}$	$4.27^{+1.33}_{-1.17}$	$2.76^{+0.86}_{-0.76}$	$3.90^{+1.22}_{-1.07}$	$5.52^{+1.72}_{-1.51}$
V1108 Her b	$0.35^{+0.08}_{-0.08}$	$0.49^{+0.12}_{-0.11}$	$0.70^{+0.17}_{-0.15}$	$0.89^{+0.21}_{-0.19}$	$1.31^{+0.32}_{-0.28}$	$1.86^{+0.45}_{-0.40}$	$1.05^{+0.25}_{-0.23}$	$1.56^{+0.38}_{-0.34}$	$2.20^{+0.53}_{-0.48}$	$2.10^{+0.51}_{-0.46}$	$2.97^{+0.72}_{-0.65}$	$4.21^{+1.02}_{-0.91}$	$2.72^{+0.66}_{-0.59}$	$3.85^{+0.93}_{-0.83}$	$5.44^{+1.32}_{-1.18}$
V592 Her b	$0.05^{+0.02}_{-0.01}$	$0.07^{+0.02}_{-0.02}$	$0.09^{+0.03}_{-0.02}$	$0.12^{+0.04}_{-0.03}$	$0.18^{+0.06}_{-0.04}$	$0.25^{+0.08}_{-0.06}$	$0.14^{+0.04}_{-0.04}$	$0.21^{+0.07}_{-0.05}$	$0.30^{+0.09}_{-0.07}$	$0.28^{+0.09}_{-0.07}$	$0.40^{+0.13}_{-0.10}$	$0.56^{+0.18}_{-0.14}$	$0.36^{+0.12}_{-0.09}$	$0.51^{+0.16}_{-0.13}$	$0.73^{+0.23}_{-0.18}$
WD 1202-024 b	$0.07^{+0.02}_{-0.02}$	$0.10^{+0.03}_{-0.03}$	$0.14^{+0.04}_{-0.04}$	$0.17^{+0.05}_{-0.04}$	$0.25^{+0.08}_{-0.07}$	$0.36^{+0.11}_{-0.09}$	$0.20^{+0.06}_{-0.05}$	$0.30^{+0.09}_{-0.08}$	$0.42^{+0.13}_{-0.11}$	$0.40^{+0.12}_{-0.10}$	$0.56^{+0.17}_{-0.14}$	$0.79^{+0.24}_{-0.20}$	$0.49^{+0.15}_{-0.13}$	$0.70^{+0.21}_{-0.18}$	$0.99^{+0.30}_{-0.26}$
WD J1820 b	$0.13^{+0.14}_{-0.09}$	$0.18^{+0.19}_{-0.12}$	$0.26^{+0.28}_{-0.18}$	$0.34^{+0.36}_{-0.23}$	$0.50^{+0.52}_{-0.33}$	$0.70^{+0.74}_{-0.47}$	$0.40^{+0.42}_{-0.27}$	$0.59^{+0.62}_{-0.40}$	$0.84^{+0.88}_{-0.56}$	$0.83^{+0.88}_{-0.56}$	$1.18^{+1.24}_{-0.79}$	$1.67^{+1.76}_{-1.12}$	$1.12^{+1.18}_{-0.75}$	$1.59^{+1.67}_{-1.07}$	$2.25^{+2.37}_{-1.51}$
WZ Sge b	$1.42^{+0.23}_{-0.22}$	$2.01^{+0.32}_{-0.30}$	$2.86^{+0.46}_{-0.43}$	$3.62^{+0.59}_{-0.55}$	$5.35^{+0.86}_{-0.81}$	$7.57^{+1.22}_{-1.15}$	$4.26^{+0.69}_{-0.65}$	$6.34^{+1.02}_{-0.96}$	$8.97^{+1.45}_{-1.36}$	$8.57^{+1.38}_{-1.30}$	$12.12^{+1.96}_{-1.84}$	$17.14^{+2.77}_{-2.60}$	$11.08^{+1.79}_{-1.68}$	$15.66^{+2.53}_{-2.37}$	$22.15^{+3.58}_{-3.36}$
ZTF J0003+14 b	$0.21^{+0.20}_{-0.13}$	$0.30^{+0.29}_{-0.18}$	$0.42^{+0.40}_{-0.26}$	$0.45^{+0.44}_{-0.28}$	$0.71^{+0.68}_{-0.44}$	$1.00^{+0.96}_{-0.62}$	$0.55^{+0.53}_{-0.34}$	$0.81^{+0.78}_{-0.50}$	$1.14^{+1.10}_{-0.71}$	$1.05^{+1.01}_{-0.65}$	$1.48^{+1.43}_{-0.92}$	$2.10^{+2.02}_{-1.30}$	$1.24^{+1.19}_{-0.77}$	$1.75^{+1.69}_{-1.08}$	$2.47^{+2.39}_{-1.53}$
ZTF J0220+21 b	$0.14^{+0.10}_{-0.07}$	$0.20^{+0.15}_{-0.10}$	$0.29^{+0.21}_{-0.14}$	$0.30^{+0.22}_{-0.15}$	$0.48^{+0.34}_{-0.24}$	$0.68^{+0.49}_{-0.34}$	$0.37^{+0.27}_{-0.18}$	$0.54^{+0.39}_{-0.27}$	$0.77^{+0.55}_{-0.38}$	$0.70^{+0.51}_{-0.35}$	$1.00^{+0.72}_{-0.50}$	$1.41^{+1.01}_{-0.70}$	$0.82^{+0.59}_{-0.41}$	$1.17^{+0.84}_{-0.58}$	$1.65^{+1.19}_{-0.82}$
ZTF J0407-00 b	$0.25^{+0.13}_{-0.10}$	$0.36^{+0.18}_{-0.14}$	$0.51^{+0.25}_{-0.20}$	$0.41^{+0.21}_{-0.16}$	$0.76^{+0.38}_{-0.30}$	$1.08^{+0.53}_{-0.42}$	$0.53^{+0.26}_{-0.21}$	$0.79^{+0.39}_{-0.31}$	$1.11^{+0.55}_{-0.44}$	$0.99^{+0.49}_{-0.39}$	$1.40^{+0.69}_{-0.55}$	$1.97^{+0.98}_{-0.77}$	$1.08^{+0.53}_{-0.42}$	$1.53^{+0.76}_{-0.60}$	$2.16^{+1.07}_{-0.85}$
ZTF J1637+49 b	$0.28^{+0.12}_{-0.10}$	$0.40^{+0.17}_{-0.14}$	$0.57^{+0.24}_{-0.20}$	$0.65^{+0.28}_{-0.23}$	$0.99^{+0.42}_{-0.35}$	$1.40^{+0.60}_{-0.49}$	$0.78^{+0.33}_{-0.27}$	$1.15^{+0.49}_{-0.40}$	$1.63^{+0.69}_{-0.57}$	$1.50^{+0.64}_{-0.52}$	$2.12^{+0.90}_{-0.74}$	$3.00^{+1.28}_{-1.05}$	$1.81^{+0.77}_{-0.63}$	$2.56^{+1.09}_{-0.89}$	$3.61^{+1.54}_{-1.26}$
ZTF J2252-05 b	$0.43^{+0.23}_{-0.17}$	$0.60^{+0.32}_{-0.24}$	$0.85^{+0.46}_{-0.34}$	$0.72^{+0.39}_{-0.29}$	$1.29^{+0.70}_{-0.52}$	$1.83^{+0.98}_{-0.73}$	$0.91^{+0.49}_{-0.37}$	$1.35^{+0.73}_{-0.54}$	$1.91^{+1.03}_{-0.77}$	$1.71^{+0.92}_{-0.69}$	$2.42^{+1.31}_{-0.98}$	$3.43^{+1.85}_{-1.38}$	$1.89^{+1.02}_{-0.76}$	$2.67^{+1.44}_{-1.07}$	$3.78^{+2.04}_{-1.52}$
Gaia 19cwm b	$0.25^{+0.07}_{-0.06}$	$0.35^{+0.10}_{-0.09}$	$0.50^{+0.14}_{-0.12}$	$0.64^{+0.18}_{-0.16}$	$0.94^{+0.27}_{-0.23}$	$1.33^{+0.38}_{-0.32}$	$0.75^{+0.21}_{-0.18}$	$1.11^{+0.32}_{-0.27}$	$1.57^{+0.45}_{-0.38}$	$1.52^{+0.43}_{-0.37}$	$2.16^{+0.62}_{-0.53}$	$3.05^{+0.87}_{-0.75}$	$2.00^{+0.57}_{-0.49}$	$2.83^{+0.81}_{-0.69}$	$4.00^{+1.14}_{-0.98}$
Gaia14aae b	$0.42^{+0.04}_{-0.03}$	$0.60^{+0.05}_{-0.05}$	$0.84^{+0.07}_{-0.07}$	$0.86^{+0.07}_{-0.07}$	$1.38^{+0.12}_{-0.11}$	$1.95^{+0.17}_{-0.16}$	$1.06^{+0.09}_{-0.09}$	$1.54^{+0.13}_{-0.13}$	$2.18^{+0.19}_{-0.18}$	$2.00^{+0.17}_{-0.16}$	$2.83^{+0.24}_{-0.23}$	$4.00^{+0.34}_{-0.33}$	$2.31^{+0.20}_{-0.19}$	$3.26^{+0.28}_{-0.27}$	$4.61^{+0.40}_{-0.38}$